SUPPORT AND ALIGNMENT

D. Connell, W. B. Herrmannsfeldt, Editor, M. J. Lee, A. V. Lisin, J. G. Niforopulos, R. C. Sandkuhle, K. Skarpaas, J. J. Spranza, K. R. Trigger, and J. K. Witthaus

This chapter describes the support and alignment systems for both the accelerator and the beam switchyard (BSY). It is divided into three parts which describe successively the laser alignment system, the accelerator support system, and the BSY support and alignment system. The purpose of these systems is to make precision mechanical adjustments for all the beam-carrying elements of the accelerator and the BSY. Thus, the systems include both the measurement and the adjustment features necessary to meet the design tolerances for alignment.

22-1 The laser alignment system (WBH, MJL, JJS, KRT)

Accurate optical alignment over very long lengths requires optics of high resolution and the elimination of atmospheric disturbance. A system of 277 large, long focal length, rectangular Fresnel lenses is used for the alignment of the accelerator. The lenses, also called targets below, are enclosed in a 24-in. diameter vacuum pipe. The system consists of a light source, a detector, and the lenses, one of which is located at each point which is to be aligned.

The tolerance for the alignment of the target points along the accelerator is ± 0.01 in. Conventional optical tooling techniques would require that a very large telescope be pointed at a reference target at the end of the accelerator. The telescope would then have to remain stable until a target at the point to be aligned could be inserted and viewed. The stability requirement would be 0.01 in./120,000 in. or less than 10^{-7} radian, a virtually impossible tolerance.

The three-point method which has been adopted eliminates the high pointing accuracy requirement. Instead, a diverging monochromatic light

source at one end of the accelerator is used to illuminate fully the target of which the position is to be determined. The target, which functions as a simple converging lens, focuses the light source to an image at the opposite end of the accelerator from the source.

The basic idea of the SLAC alignment system is illustrated in Fig. 22-1. A straight line is defined between a point source of light (L) and a detector (D). The light source is a helium–neon laser. The detector consists of a mechanical scanning system and a photomultiplier with suitable output equipment capable of resolving a shift of 0.001 in. at any of the accelerator support points. The actual sensitivity or least-count of the detector is one-tenth of that, or ± 0.0001 in. At each support point, a target T is supported on a remotely actuated hinge. Three additional targets are mounted on monuments, such as the one at M, which are 24-in. diameter pillars supported by rock below the accelerator foundation. To check the alignment at a desired point, the target at that point is inserted into the light beam by actuating the hinge mechanism. The target is actually a rectangular Fresnel lens with the correct focal length so that an image of the light source is formed on the plane of the detector. This image is then scanned by the detector in both the vertical and the horizontal directions to determine the displacement of the lens from the predetermined line.

The lenses are mounted in a 24-in. diameter aluminum pipe (see Fig. 22-2) which is the basic support girder for the accelerator. The support girder is evacuated to about 10^{-2} torr to prevent air refraction effects from distorting or deflecting the alignment image. If any adjustments are required, the support girder is moved by means of a pair of vertical screw jacks and a sidewall screw jack.

The accelerator proper is mounted about 27 in. above the center of the support girder. Because the optical alignment system is only intended to align the support girder in the horizontal and vertical directions, it is necessary to provide an auxiliary system of levels to prevent azimuthal misalignment

Figure 22-1 Schematic diagram of the two-mile linear accelerator alignment light pipe showing position of Fresnel lenses in light pipe girders and monument box.

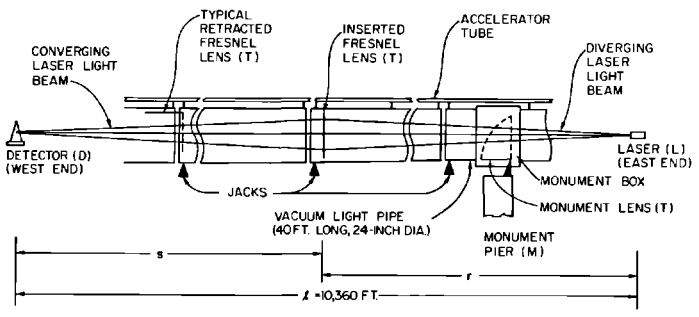

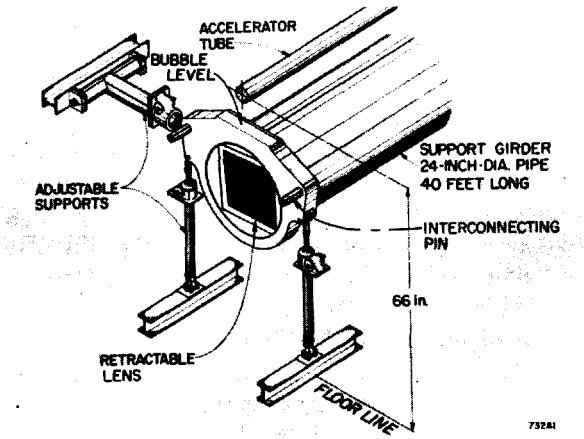

Figure 22-2 Components of alignment system showing the mounting arrangement at the lens end of each accelerator support girder. The lens is shown in the "inserted" position. When "retracted," the lens is in a horizontal position near the top of the pipe.

of the support girder which, to first order, would have the effect of horizontal misalignment of the accelerator. The azimuthal tolerance is about 1 min of arc. Fig. 5-15 is a photograph of an installed 40-ft. accelerator module before the preceding module was moved into place.

The standard accelerator module consists of four 10-ft. long sections of disk-loaded waveguide mounted on top of a 40-ft long section of the 24-in. diameter aluminum support girder. At the end of each sector, which consists of eight 40-ft long modules, there is a special 9-ft long drift section used for steering, focusing, and instrumentation. The standard drift section consists of focusing and steering magnets, beam monitoring devices, and a 0.62-in. diameter collimator, all of which are mounted on a 9-ft long section of support girder. There is a total of thirty such sectors, i.e., 240 of the 40-ft modules and thirty of the 9-ft drift sections, plus three extra modules for the injector and the positron source. As described above, each module is supported at the input end by a pair of precision screw jacks from the floor and by a third jack from the wall, as shown in Fig. 22-2. The output end of a module is attached to the beginning of the next module by a pair of heavy guide pins which allow for thermal expansion. Both the support girders themselves and the four 10-ft long accelerator sections supported by each of them are joined end-to-end by heliarc-welded bellows. A 3-in. thick aluminum end flange is welded to the input end of each section of support girder. The connecting pins from the three jacks are fastened to the outside of this flange. The lens hinge assembly is mounted at the top of the inside of the flange. The accelerator sections are supported on adjustable brackets along the support girder,

except for the first support bracket for the first section. This bracket, which begins above the 3-in. flange, is pinned in place. The whole design of the input flange is intended to provide maximum rigidity between the accelerator sections and the alignment lens.

The alignment lens is mounted on a 14-in. square stainless steel frame. The hinged support plate is spring-loaded to hold the lens firmly against the lower stop when it is inserted in the light beam. A spring-loaded actuator holds the lens horizontally against the top of the support girder, when it is not being used. In this position the lens is hidden behind a square baffle which is mounted in the output end of the adjacent support girder segment. During alignment, one lens at a time is inserted in the light beam produced by the laser. The insertion is obtained by operating a bellows actuator which is mounted in an opening at the top of the support girder. The control panel for the lens actuator is in the klystron gallery directly above the accelerator. Indicator lights wired to microswitches within the support girder show the position of the lens to the operator in the klystron gallery. In addition, the operator of the detection equipment at the end of the accelerator has an indicator showing if any lens in the entire system is not fully retracted. This indicator assures the operator that only one lens at a time is affecting the pattern of the image being viewed. The operator also has control switches to permit him to insert one lens at each drift section in order to make a quick survey of the key points along the accelerator.

Light source

The light source for the alignment system is a standard model commercial helium–neon gas laser. The lenses are designed for the fundamental visible wavelength of 6328 Å. A glass lens of short focal length is mounted on the laser to cause the beam to diverge sufficiently to illuminate fully the closest Fresnel lens, which is about 50 ft away. This lens has a diagonal dimension of about 6 in., but to insure that it is evenly illuminated and further to reduce the pointing requirement, the beam is diverged to about twice that diameter. Even with the diverging lens, the intensity of the images on a ground glass screen is sufficient to be viewed in subdued light. The laser output is from 1.0 to 3.0 mW.

Lens design and fabrication

The targets are rectangular Fresnel-zone plates made out of nickel plated copper. The rectangular design was preferred over the classical circular zone plate primarily for reasons of fabrication. It is easier to rule straight lines than circles, and the circular zones would have required special spiders for supports. The basic scheme would, of course, also have worked with glass lenses. The overwhelming objection to glass was that ordinary glass turns dark in high radiation fields such as are found along the accelerator. Also,

the cost for glass lenses, particularly of radiation-resistant material, would have been much greater.

The one-dimensional Fresnel pattern is shown in Fig. 22-3. The distance from the center line of the target to the nth slot is

$$X_n = \left(\frac{\lambda rs}{2l}\right)^{1/2} (4n)^{1/2} \tag{22-1}$$

This expression is the same as that derived for the radius of the $2n$ Fresnel zone in most standard optics texts.[1] In it, λ is the wavelength, r and s are, respectively, the distances from the lens to the laser and to the detector, and $l = r + s$ (See Fig. 22-1). The edges of the nth slot are at

$$X_{ni} = \left(\frac{\lambda rs}{2l}\right)^{1/2} (4n + d - 1)^{1/2}$$

and

$$X_{no} = \left(\frac{\lambda rs}{2l}\right)^{1/2} (4n + d + 1)^{1/2} \tag{22-2}$$

The subscripts "i" and "o" denote the inner and outer edges of a slot, respectively. The arbitrary constant d selects the point at which the slot edges are located in each Fresnel zone. For example, the values 0.0 and 2.0

Figure 22-3 One-dimensional Fresnel pattern. The spacing is the same as for a circular Fresnel lens with the same product of focal length and wavelength.

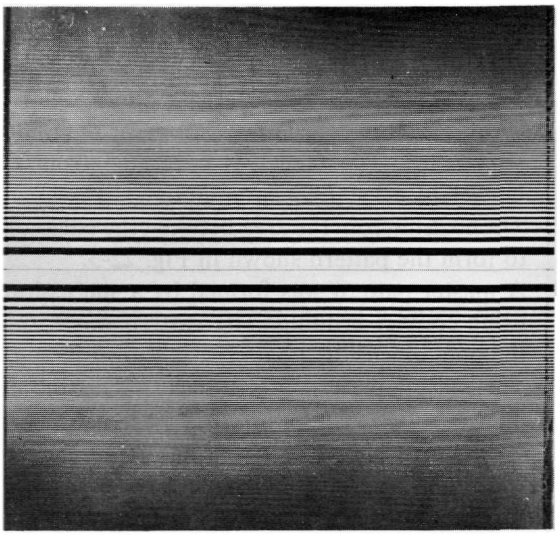

248-4-A

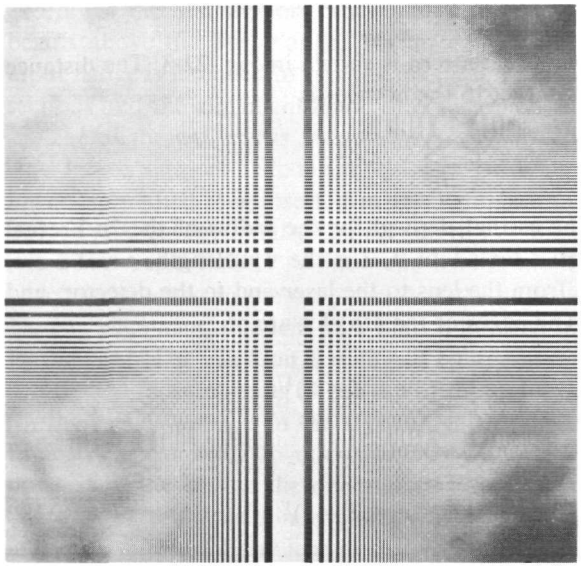

Figure 22-4 Crossed pattern of the rectangular Fresnel lens. The actual lenses have open spaces in the dark areas. The opaque center ribbon, 0.4 in. in width, provides added structural support.

for d have the effect of making two patterns which are inverse or negatives of each other.

The targets are formed by chemically milling an array of rectangular holes into a copper sheet which is about 14 in. square and 0.02 in. thick. The following step-by-step process was developed by the manufacturer*:

1. The complete one-dimensional pattern was ruled on a coated glass plate with an automatic diamond-tipped ruling engine controlled by punched paper tape. The tape was generated from the output of the Stanford University IBM 7090 computer.
2. The coating from the area between the edges of the open slots was stripped to form the pattern shown in Fig. 22-3.
3. A master pattern was formed by a succession of photographic steps, all using contact printing. The pattern was formed from crossed images of the one-dimensional pattern, as shown in Fig. 22-4.
4. The master pattern was transferred to the copper sheet by applying a light-sensitive coating known as photoresist and by exposing the coated copper to the master pattern. The nature of the photoresist coating is

* Metrigraphics Laboratories, Division of Dynamics Research Corporation, Stoneham, Massachusetts.

such that, after developing and fixing, it is possible to use a suitable solvent to wash away the coating where it has been exposed to light. The resulting areas of clean copper may then be used for subsequent plating or etching operations.

5. A 0.002-in. thick layer of nickel was electroplated on the clean copper to form the actual pattern of the target.
6. By chemical milling, the unplated copper was removed to form the required pattern of holes as shown in Fig. 22-4. The chemical milling process was controlled to retain the copper behind the nickel plating wherever possible. Generally, some copper remains if the width of the ribbon is greater than the thickness of the copper sheet.
7. A thin flash-coating of nickel for protection was applied to the target which now resembles the cross-sectional view shown in Fig. 22-5.
8. The target was mounted on the stainless steel frame by match-drilling the target and the frame. The frame has a pair of holes which fit over locating pins on the target hinge, thus completing the connection between the target and the accelerator.

Errors in the position of the edges of the apertures can always be divided into symmetric and asymmetric components. The maximum error that can occur in finding the center of the target is essentially the magnitude of the asymmetric shift of the aperture edges. This conclusion was verified by calculations based on methods which will be used later in this paper. The calculations are detailed in an internal document.[2] The tolerance for the aperture edges is 0.001 in. which is the same as the criterion for the sensitivity of alignment of each lens.

Symmetric errors can only affect the intensity and sharpness of the image, not its position. The only important type of symmetric error is that which is proportional to the distance of the edge of the aperture from the center of the target. This error is equivalent to having the wrong focal length for the target as calculated from Eq. (22-2) where the focal length f is given by $f = rs/l$. The longitudinal distance by which each target can be moved without causing a reduction in alignment sensitivity greater than 10% has been calculated by a digital computer program. In many cases it was found possible to let one target pattern be used in two or more positions without exceeding the 10% limitation. In addition, it was frequently possible to use the same

Figure 22-5 Cross section of a target showing how the apertures are formed by the 0.002-in. thick nickel plating on 0.02-in. thick copper sheets. Where the holes are small and closely spaced, all the copper was often etched away.

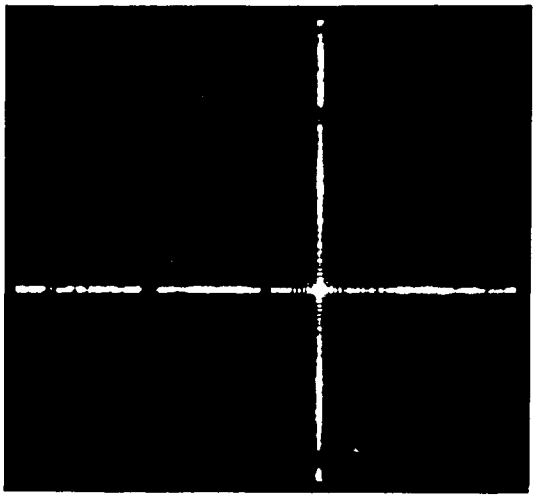

ACTUAL SIZE

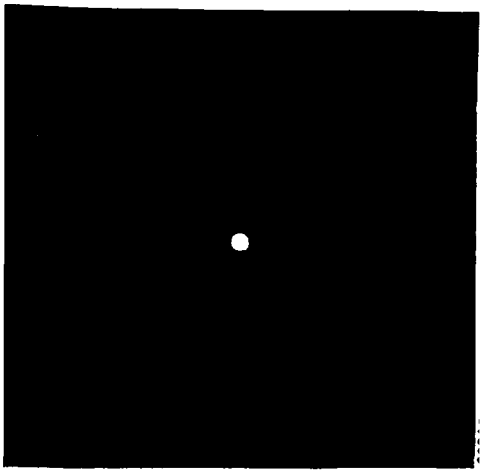

ENLARGED

Figure 22-6a Photograph of image pattern from a Fresnel lens 1000 ft from the focal plane. The point to be aligned is the spot at the center of the crossed lines. The width of the center spot corresponds to the diffraction limit of the Fresnel lens.

target at an exactly symmetrically located position relative to the center of the accelerator. This is equivalent to exchanging r and s in Eq. (22-2). As a result, a total of only 121 different patterns was required for the 277 target locations along the accelerator.

Most of the patterns are 12 in. square. However, a limit of 250 slots was set for ease of fabrication, and as a result, at the ends of the accelerator the targets have 250 lines in less than 12 in. The smallest of the targets, which is the very last one, is only about 4 in. square. The smallest slot in this last target is about 0.004 in. wide. The target with the longest focal length, which is located at the center of the accelerator, has only forty-six slots in each direction of the 12 in. square.

Detector

The spot or line width of the image at the detection station varies from about 0.004 in. for the last target to about 0.5 in. for the target nearest the light source. Figures 22-6a and b show photographs of a typical image pattern. The most difficult targets to align are the ones in the center of the accelerator. In this region, line widths are about 0.2 in. The desired resolution of the alignment system is 0.001 in. With a 2 : 1 enlargement ratio of a lens in the center of the accelerator, it is necessary to find the center of the spot within

Figure 22-6b Photograph of image pattern from a Fresnel lens 9000 ft from the focal plane. The point to be aligned is the spot at the center of the crossed lines. The width of the center spot corresponds to the diffraction limit of the Fresnel lens.

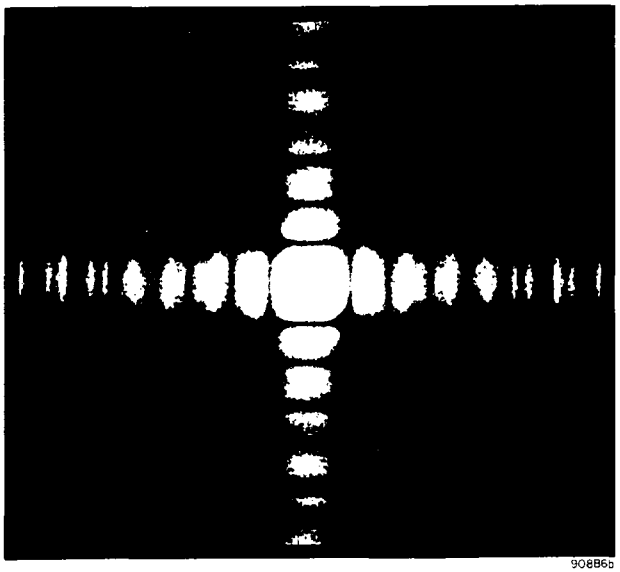

908B6b

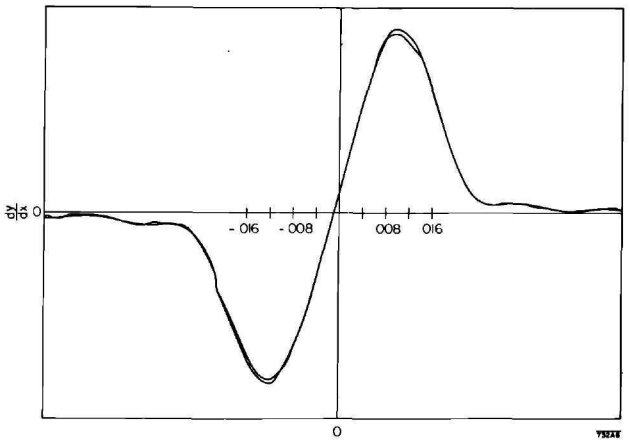

Figure 22-7 Plot of the differentiated signal from the photoelectric scanner. The trace was repeated to show the reproducibility of the output.

0.002 in. or 1 part in 100 of the line width. This is better than a human operator could be expected to do routinely. Therefore, an electromechanical scanning system has been devised which generates the derivative of the spot intensity as a function of detector position in the horizontal and vertical directions. The center of the spot is defined by the point where the derivative is zero. The advantage of using this method is that the steep derivative line intersecting the axis gives an unambiguous determination of the image center. Figure 22-7 shows the actual plot of the differentiated alignment image as obtained from an *x-y* recorder. The curve was traced twice to establish the reproducibility of the results. Figure 22-8 shows an artist's cutaway

Figure 22-8 Variable-amplitude scanner and photomultiplier. The scanner may be rotated to sweep either vertically or horizontally.

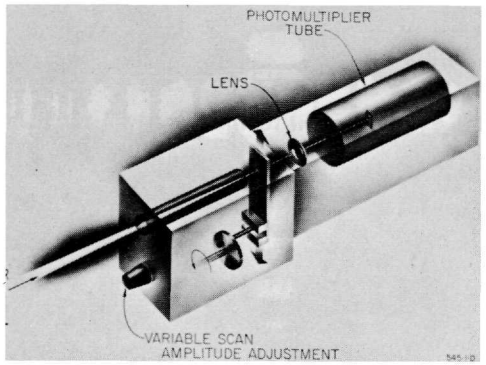

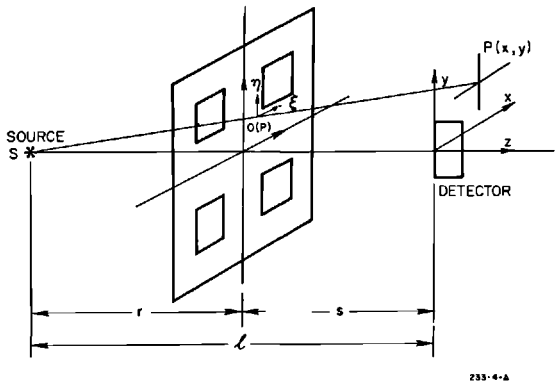

Figure 22-9 Coordinate system for calculating the Fresnel integrals. The amplitude U(P) at the detector is found by integrating from the point O(P) on the target.

of the detector assembly. The detector can be rotated so that it can scan either horizontally or vertically. A switching mirror system at the detector permits the operator to view the image on a ground glass or to direct it into the detector.

Referring to Fig. 22-7, the slope of the trace as it crosses the horizontal axis is proportional to the second derivative of the intensity at the peak of the image spot (d^2I/dx^2), where x is the transverse displacement in the image plane, as shown in Fig. 22-9. When the second derivative of the intensity curve is multiplied by the peak intensity I_0, a measure of the error signal as a function of displacement of the image is obtained. When the square root of this quantity is multiplied by the magnification of the system, l/r, the resulting product is proportional to the signal obtained by displacing the target, thus giving as a measure of the alignment sensitivity

$$\frac{d}{dx}(\text{output signal}) \text{ which is proportional to } \left[I_0\left(\frac{d^2I}{dx^2}\right)\right]^{1/2}_{x=0}\left(\frac{l}{r}\right) \quad (22\text{-}3)$$

Image pattern

The calculation of the image intensity from a pattern of holes in a target plate involves the use of Fresnel integrals. Both Taylor series approximations of the integrals and digital computer programs have been used for calculating the expected images. The analytical approximations will be presented below for the rectangular Fresnel lens.

Referring to Fig. 22-9, the intensity at any point P on the image plane of light which has passed through an arbitrary hole pattern is

$$I(P) = |U(P)|^2 \quad (22\text{-}4)$$

For a point source S, the amplitude $U(P)$ is given by the Fresnel-Kirchoff diffraction integral which, to second order in the variables ξ and η describing the surface is

$$U(P) = \frac{-iAe^{ikl}}{2l} \iint_{\text{target}} \exp\left[i\frac{\pi}{2}(\mu^2 + v^2)\right] d\mu\, dv \tag{22-5}$$

where μ and v are the normalized distances from the origin P on the target and are given by

$$\mu^2 = \frac{2l}{\lambda rs}\xi^2 \qquad \text{and} \qquad v^2 = \frac{2l}{\lambda rs}\eta^2 \tag{22-6}$$

The wave number is $k = 2\pi/\lambda$ and, as in Fig. 22-9, r and s are the source and image distances, respectively, and $l = r + s$. The point $O(P)$ is the point where the line joining S and P intersects the plane of the target. The source intensity is A^2 units-of-power per steradian.

By taking coordinates ξ and η parallel to the edges of the holes, the integrals in Eq. (22-5) can be separated, giving

$$U(P) = \frac{-iAe^{ikl}}{2l} \int_{\mu} e^{i(\pi/2)\mu^2}\, d\mu \int_{v} e^{i(\pi/2)v^2}\, dv \tag{22-7}$$

Substituting Eq. (22-7) back into Eq. (22-4), the expansion for $I(P)$ becomes

$$\begin{aligned} I(P) &= \left(\frac{A}{2l}\right)^2 \{C^2[\mu(P)] + S^2[\mu(P)]\} \cdot \{C^2[v(P)] + S^2[v(P)]\} \\ &= \left(\frac{A}{2l}\right)^2 I_\mu I_v \end{aligned} \tag{22-8}$$

There are a variety of ways to design the target within the mechanical limitations. A simple illustration is to attempt to maximize the C integrals while minimizing the S integrals for $P = 0$. If we write

$$C(0) = \int \cos\left(\frac{\pi}{2}\mu^2\right) d\mu$$

and

$$S(0) = \int \sin\left(\frac{\pi}{2}\mu^2\right) d\mu \tag{22-9}$$

and allow slots at $(4n-1) < \mu^2 < (4n+1)$ and ribbons at $(4n+1) < \mu^2 < (4n+3)$, the $\cos[(\pi/2)\mu^2]$ function will always be positive during intervals of contribution to the integral while the $\sin[(\pi/2)\mu^2]$ function will oscillate in a manner that causes the integral to be small. The nth slot will then have edges at

$$\xi_+ = \left(\frac{\lambda rs}{2l}\right)^{1/2}(4n+1)^{1/2}$$

and

$$\xi_- = \left(\frac{\lambda rs}{2l}\right)^{1/2}(4n-1)^{1/2} \tag{22-10}$$

In the case of the targets for the main part of the accelerator, a support strip was required through the middle of each target. This prevented inclusion of the center or $n = 0$ slot. The best alternative was to make the central ribbon the same width (0.4 in.) in all targets. Under this condition, the slot edges as defined by Eq. (22-10) do not give optimum peak intensity. It is shown in the Appendix to this chapter that the peak intensity can be maximized by the addition of the constant d under the radical as in Eq. (22-2), with the value of d determined for each target by the central ribbon width. Since $\lambda rs/2l = \lambda f/2$ is different for each target, it is necessary to calculate d from the expression in Eq. (22-2) for the inner edge of the first slot $X_{1i}^2 = (\lambda f/2)(3+d)$, yielding

$$d = \frac{X_{1i}^2}{(\lambda f/2)} - 3 \tag{22-11}$$

where the value for X_{1i} is the half-width of the ribbon, 0.2 in. For the present example, the case for $d = 0$ as in Eq. (22-10), will be considered further, but without the center slot.

Having defined the target pattern as alternating slots and ribbons, the integrals can be rewritten as sums of integrals over the successive slots. Thus,

$$C(\varepsilon) = \sum_{\substack{n=-N \\ n\neq 0}}^{N} \int_{\mu_{n-}(\varepsilon)}^{\mu_{n+}(\varepsilon)} \cos\left(\frac{\pi}{2}t^2\right) dt \tag{22-12}$$

and

$$S(\varepsilon) = \sum_{\substack{n=-N \\ n\neq 0}}^{N} \int_{\mu_{n-}(\varepsilon)}^{\mu_{n+}(\varepsilon)} \sin\left(\frac{\pi}{2}t^2\right) dt \tag{22-13}$$

where ε is the normalized displacement from P at the point where the line from S to the point of interest on the image plane crosses the target. Thus, for the intensity at the peak, the integrals are evaluated for $\varepsilon = 0$. By

measuring ε in the normalized coordinates, as in Eq. (22-6), the slot edges, which are the limits of integration, become

$$\mu_{n-}(\varepsilon) = (4n - 1)^{1/2} - \varepsilon$$

and

$$\mu_{n+}(\varepsilon) = (4n + 1)^{1/2} - \varepsilon \tag{22-14}$$

for $n > 0$, and

$$\mu_{n-}(\varepsilon) = -(4|n| + 1)^{1/2} - \varepsilon$$

and

$$\mu_{n+}(\varepsilon) = -(4|n| - 1)^{1/2} - \varepsilon$$

for $n < 0$.

To analyze the intensity of the image near the central maximum, the one-dimensional intensity of Eq. (22-8) is expressed as a power series in ε. This results in

$$I_\mu(\varepsilon) = C^2(0) + S^2(0) + \varepsilon\left[2C\frac{\partial C}{\partial \varepsilon} + 2S\frac{\partial S}{\partial \varepsilon}\right]_{\varepsilon=0} + \frac{\varepsilon^2}{2}\left[2\left(\frac{\partial C}{\partial \varepsilon}\right)^2 + 2C\frac{\partial^2 C}{\partial \varepsilon^2} + 2\left(\frac{\partial S}{\partial \varepsilon}\right)^2 + 2S\frac{\partial^2 S}{\partial \varepsilon^2}\right]_{\varepsilon=0} + \cdots \tag{22-15}$$

where

$$\frac{\partial C}{\partial \varepsilon} = -\sum_n \left[\cos\left(\frac{\pi}{2}\mu_{n+}^2\right) - \cos\left(\frac{\pi}{2}\mu_{n-}^2\right)\right]$$

$$\frac{\partial^2 C}{\partial \varepsilon^2} = -\pi\sum_n \left[\mu_{n+}\sin\left(\frac{\pi}{2}\mu_{n+}^2\right) - \mu_{n-}\sin\left(\frac{\pi}{2}\mu_{n-}^2\right)\right]$$

$$\frac{\partial S}{\partial \varepsilon} = -\sum_n \left[\sin\left(\frac{\pi}{2}\mu_{n+}^2\right) - \sin\left(\frac{\pi}{2}\mu_{n-}^2\right)\right]$$

and

$$\frac{\partial^2 S}{\partial \varepsilon^2} = \pi\sum_n \left[\mu_{n+}\cos\left(\frac{\pi}{2}\mu_{n+}^2\right) - \mu_{n-}\cos\left(\frac{\pi}{2}\mu_{n-}^2\right)\right]$$

For the range of boundaries of interest, good approximations for the integrals are[3]

$$\int_0^\mu \cos\left(\frac{\pi}{2}t^2\right)dt \approx \frac{1}{2} - \frac{1}{\pi\mu}\left[\frac{\cos\left(\frac{\pi}{2}\mu^2\right)}{\pi\mu^2} - \sin\left(\frac{\pi}{2}\mu^2\right)\right] \tag{22-16}$$

and

$$\int_0^\mu \sin\left(\frac{\pi}{2}t^2\right)dt \approx \frac{1}{2} - \frac{1}{\pi\mu}\left[\frac{\sin\left(\frac{\pi}{2}\mu^2\right)}{\pi\mu^2} - \cos\left(\frac{\pi}{2}\mu^2\right)\right] \tag{22-17}$$

Using Eq. (22-16),

$$C(0) = \sum_{1}^{N} \int_{\mu_{n-}}^{\mu_{n+}} \cos\left(\frac{\pi}{2} t^2\right) dt + \sum_{-1}^{-N} \int_{\mu_{n-}}^{\mu_{n+}} \cos\left(\frac{\pi}{2} t^2\right) dt$$

$$= \frac{1}{\pi}\left[\sum_{1}^{N} \left\{\frac{\pi}{2} - \frac{\cos\left(\frac{\pi}{2}\right)\mu^2}{\pi\mu^3} + \frac{\sin\left(\frac{\pi}{2}\right)\mu^2}{\mu}\right\}_{(4n-1)^{1/2}}^{(4n+1)^{1/2}}\right.$$

$$\left. + \sum_{-1}^{-N} \left\{\frac{\pi}{2} - \frac{\cos\left(\frac{\pi}{2}\mu^2\right)}{\pi\mu^3} + \frac{\sin\left(\frac{\pi}{2}\mu^2\right)}{\mu}\right\}_{-(4|n|+1)^{1/2}}^{-(4|n|-1)^{1/2}}\right]$$

$$= \frac{2}{\pi} \sum_{1}^{N} [(4n+1)^{-1/2} + (4n-1)^{-1/2}] \approx \frac{2}{\pi} \sum_{1}^{N} n^{-1/2} \qquad (22\text{-}18)$$

Similarly, it can be shown that

$$S(0) \approx -\frac{2}{\pi^2} \sum_{1}^{N} [(4n+1)^{-3/2} + (4n-1)^{-3/2}] \approx \frac{-1}{2\pi^2} \sum_{1}^{N} n^{-3/2} \qquad (22\text{-}19)$$

Except for small values of N, the contribution of $S^2(0)$ to $I_\mu(0)$ is negligible. The sum in Eq. (22-18) can be approximated by

$$\sum_{1}^{N} n^{-1/2} \approx \frac{1}{2}\left[\int_{2}^{N+1} n^{-1/2}\, dn + \int_{2}^{N+1} (n-1)^{-1/2}\, dn\right] + 1$$

$$= (N+1)^{1/2} + N^{1/2} - 2^{1/2} \qquad (22\text{-}20)$$

Thus $C^2(0)$ may be expressed as

$$C^2(0) = \frac{4}{\pi^2}[(N+1)^{1/2} + N^{1/2} - 2^{1/2}]^2 \qquad (22\text{-}21)$$

which agrees with computer calculations of $I(0)$ within 0.25% for $N > 25$.

In completing the expansion to second order for Eq. (22-15) using the above method, it is found that

$$\left.\frac{\partial C}{\partial \varepsilon}\right|_0 = \left.\frac{\partial S}{\partial \varepsilon}\right|_0 = \left.\frac{\partial^2 S}{\partial \varepsilon^2}\right|_0 = 0 \qquad (22\text{-}22)$$

The only nonzero term for second order is

$$\frac{\partial^2 C}{\partial \varepsilon^2} = -2\pi \sum_{1}^{N} [(4n+1)^{1/2} + (4n-1)^{1/2}] \approx -8\pi \sum_{1}^{N} n^{1/2}$$

$$\approx -4\pi\left[\int_{1}^{N+1} n^{1/2}\, dn + \int_{1}^{N+1} (n-1)^{1/2}\, dn\right]$$

$$= -\frac{8\pi}{3}[(N+1)^{3/2} + N^{3/2} - 1] \qquad (22\text{-}23)$$

Substituting Eqs. (22-21), (22-22), and (22-23) into Eq. (22-15) gives

$$I_\mu(\varepsilon) \approx \frac{4}{\pi^2}\left[(N+1)^{1/2} + N^{1/2} - 2^{1/2}\right]^2 \cdot \left[1 - \varepsilon^2 \frac{4\pi^2}{3} \frac{(N+1)^{3/2} + N^{3/2} - 1}{(N+1)^{1/2} + N^{1/2} - 2^{1/2}} + \cdots\right] \tag{22-24}$$

For an alignment target formed by superimposing identical patterns at right angles to each other, the symmetry condition

$$I_\mu(0) = I_\nu(0) \tag{22-25}$$

can be used. Then using Eq. (22-8), with $N \gg 1$, Eq. (22-24) becomes

$$I(\varepsilon) = \left(\frac{A}{l}\right)^2 \frac{64N^2}{\pi^4}\left[1 - \varepsilon^2 \frac{4\pi^2 N}{3} + \cdots\right] \tag{22-26}$$

which describes the intensity near the peak along one of the axis lines through the center.

Detector signals

The methods used to analyze the image intensity from the rectangular Fresnel lens will now be extended to study the signal from the detector. The image is scanned in one direction at a time by a linearly oscillating aperture which moves parallel to the direction in which the scanning motion is made. A phase-sensitive detector is used to analyze the signal. To get an analytical expression of the signal amplitude, slope, and line width, the image intensity will be expanded in a Taylor series.

If $H(x, y)$ describes an aperture located at x and y on the image plane, the power into a photomultiplier tube placed behind the aperture is

$$P(x, y) = \left(\frac{A}{2l}\right)^2 \int_{H(x,y)} I(\xi) I(\eta)\, d\xi\, d\eta \tag{22-27}$$

As defined in Eq. (22-6), ξ and η are measured in the target plane. $I(\xi)$ and $I(\eta)$ can be expanded in a Taylor series as

$$I(\xi) = I(0) + \xi I^{(1)} + \frac{\xi^2}{2} I^{(2)} + \cdots \tag{22-28}$$

where

$$I^{(n)} = \left.\frac{\partial^n I}{\partial \xi^n}\right|_{\xi=0}$$

It is convenient to make the calculation using a rectangular aperture with dimensions $2a$ wide by $2b$ high. Then the integral in Eq. (22-27) becomes

$$\int_{H(x\ y)} I(\xi)I(\eta)\,d\xi\,d\eta = \left(\frac{r}{l}\right)^2 \int_{x-a}^{x+a} I(\xi)\,d\xi \int_{y-b}^{y+b} I(\eta)\,d\eta \tag{22-29}$$

where the r/l factors come from measuring ξ and η at the image plane.

If the scan is made in the x-direction exactly through the peak of the image at $y = 0$, then

$$\frac{r}{l}\int_{-b}^{b} I(\eta)\,d\eta = 2I(0)b + \frac{2}{3!}I^{(2)}b^3 + \cdots = G(0) \tag{22-30}$$

and

$$\begin{aligned}\frac{r}{l}\int_{x-a}^{x+a} I(\xi)\,d\xi &= 2I(0)a + \frac{1}{2}[(x+a)^2 - (x-a)^2]I^{(1)} \\ &\quad + \frac{1}{3!}[(x+a)^3 - (x-a)^3]I^{(2)} \\ &\quad + \frac{1}{4!}[(x+a)^4 - (x-a)^4]I^{(3)} \\ &\quad + \frac{1}{5!}[(x+a)^5 - (x-a)^5]I^{(4)} \\ &\quad + \cdots \\ &= 2I(0)a + 2xaI^{(1)} + \left(ax^2 + \frac{a^3}{3}\right)I^{(2)} \\ &\quad + \frac{xa}{3}(x^2 + a^2)I^{(3)} \\ &\quad + \frac{2a}{5!}(5x^4 + 10x^2a^2 + a^4)I^{(4)} + \cdots \\ &= F(x)\end{aligned} \tag{22-31}$$

The motion of the aperture is described by

$$x = x_0 + d\sin\omega t \tag{22-32}$$

where x_0 is the position of the center of oscillation at time t and the amplitude of oscillation is d. From Eq. (22-32),

$$\begin{aligned}x^2 &= x_0^2 + 2x_0\,d\sin\omega t + d^2\sin^2\omega t \\ x^3 &= x_0^3 + 3x_0^2\,d\sin\omega t + 3x_0\,d^2\sin^2\omega t + d^3\sin^3\omega t\end{aligned} \tag{22-33}$$

and

$$x^4 = x_0^4 + 4x_0^3\,d\sin\omega t + 6x_0^2\,d^2\sin^2\omega t + 4x_0\,d^3\sin^3\omega t + d^4\sin^4\omega t$$

The output signal can be obtained in terms of the primary oscillating frequency and harmonics by using the following standard trigonometric identities:

$$\sin^2 \omega t = \tfrac{1}{2} - \tfrac{1}{2}\cos 2\omega t$$

$$\sin^3 \omega t = \tfrac{3}{4}\sin \omega t - \tfrac{1}{4}\sin 3\omega t \tag{22-34}$$

and

$$\sin^4 \omega t = \tfrac{3}{8} - \tfrac{1}{2}\cos 2\omega t + \tfrac{1}{8}\cos 4\omega t$$

The Fourier analysis can then be made by combining Eqs. (22-31) through (22-34) and grouping terms with the same harmonic number. When this is done, the terms with the fundamental frequency are

$$\frac{l}{r}F_1(x_0) = 2I^{(1)}ad + 2I^{(2)}adx_0 + I^{(3)}a\left[x_0^2 d + \frac{a^2 d}{3} + \frac{d^3}{4}\right] + \tfrac{1}{3}I^{(4)}a[x_0^3 d + \tfrac{3}{4}x_0 d^3 + x_0 a^2 d] + \cdots \tag{22-35}$$

To evaluate Eq. (22-35), notice by comparing Eq. (22-21) and (22-24) that

$$I_\mu(\varepsilon) \approx \left[\sum_{\substack{n=-N \\ n\neq 0}}^{N} \int_{\mu_{n-}(\varepsilon)}^{\mu_{n+}(\varepsilon)} \cos\left(\frac{\pi}{2}t^2\right) dt\right]^2 = C^2(\varepsilon) \tag{22-36}$$

From the definition in Eq. (22-6) and from Eq. (22-28)

$$\frac{r}{l}I^{(n)} = \left(\frac{2r}{\lambda ls}\right)^{n/2}\frac{\partial^n I_\mu}{\partial \varepsilon^n} \tag{22-37}$$

where the derivatives are found by successive differentiation of Eq. (22-36).

The derivatives of the $C(\varepsilon)$ integrals follow the pattern used after Eq. (22-15). If the same model target that was assumed in the analysis of the rectangular Fresnel lens is used, then the limits of integration are the same as given by Eq. (22-14).

Predictably, it is found that the odd derivatives are

$$\left.\frac{\partial C}{\partial \varepsilon}\right|_{\varepsilon=0} = \left.\frac{\partial^3 C}{\partial \varepsilon^3}\right|_{\varepsilon=0} = 0 \tag{22-38}$$

$C(0)$ and $\partial^2 C/\partial\varepsilon^2|_{\varepsilon=0}$ are given by Eqs. (22-21) and (22-23), respectively. Continuing to the fourth derivative from Eq. (22-15),

$$\frac{\partial^4 C}{\partial \varepsilon^4} = \frac{32\pi^3}{5}[(N+1)^{5/2} + N^{5/2} - 1] \tag{22-39}$$

is obtained. Combining Eqs. (22-35) through (22-39), the coefficient of the fundamental frequency is found to be

$$F_1(x_0) \approx -\frac{2r}{\lambda ls}(2adx_0)\frac{128N^2}{3}\left[1 - \left(\frac{2r}{\lambda ls}\right)\left(x_0^2 + \frac{3}{4}d^2 + a^2\right)\frac{16\pi^2 N}{15} + \cdots\right] \tag{22-40}$$

The width of the image can be defined as the distance between maximum and minimum of $F_1(x_0)$. As such, it is approximately the distance between

the positive and negative peaks in Fig. 22-7 and is about equal to the full width at half-maximum. If it is assumed that a and d are small compared with the distance to the maximum or minimum, x_m, then by setting $dF_1(x_0)/(dx_0) = 0$,

$$1 - \frac{16\pi^2}{5} N x_m^2 \left(\frac{2r}{\lambda l s}\right) = 0$$

From this one finds

$$x_m = \pm \left[\frac{16\pi^2}{5} N \frac{2r}{\lambda l s}\right]^{-1/2} \tag{22-41}$$

Thus the line width, $x_{\max} - x_{\min}$, is proportional to $(Nr/s)^{-1/2}$.

In practice the light pipe has constant diameter, thus limiting the targets to a fixed maximum width. Letting $\mu^2 = 4N$ in Eq. (22-6), ξ equals the half-width of a target so that the effective width of a target is

$$D = \left(\frac{8N\lambda r s}{l}\right)^{1/2} \tag{22-42}$$

Combining Eqs. (22-41) and (22-42), the width of the image is found to be

$$w \approx \sqrt{5} \frac{\lambda s}{\pi D} \tag{22-43}$$

which, for the middle of the accelerator, is 0.17 in. Equation (22-43) is strikingly close to the standard expression for resolution of a lens, $\lambda s/D$.

The detection sensitivity is equal to the derivative of the first harmonic coefficient at $x_0 = 0$. Combining Eqs. (22-27) and (22-30) and differentiating, one obtains

$$\left.\frac{dP_1}{dx_0}\right|_{x_0=0} \approx \left(\frac{A}{2l}\right)^2 G(0) \left.\frac{dF_1}{dx_0}\right|_{x_0=0}$$

which, on substituting from Eqs. (22-30) and (22-40), becomes

$$\left.\frac{dP_1}{dx_0}\right|_{x_0=0} \approx -\left(\frac{A}{2l}\right)^2 \left(\frac{16N}{\pi^2} 2b\right)\left(\frac{2r}{\lambda l s}\right)\left(\frac{256N^2}{3} ad\right) \tag{22-44}$$

If it is assumed that the dimensions of the aperture are proportional to the image width such that $b = 2a = Dw$, where D is a constant of proportionality, Eq. (22-44) reduces to

$$\left.\frac{dP_1}{dx_0}\right|_{x_0=0} \approx -17\left(\frac{A}{2l}\right)^2 N^2 D^2 d \tag{22-45}$$

With a laser source that emits 1 mW into a solid angle of $4\pi \times 10^{-4}$ steradian, $(A/2l)^2 \approx 1.3 \times 10^{-11}$ W/in.^{2} for $l \approx 1.2 \times 10^5$ in. Assuming the sweep amplitude d of the scanner is equal to $w/2$, one finds

$$\left|\frac{dP_1}{dx}\right| \approx 1.1 \times 10^{-10} N^2 D^2 w \text{ (W/in.)}$$

In the center of the accelerator, the targets only have 46 lines, or $N = 23$. Putting $D = 1/10$, $|dP_1/dx| \approx 1 \times 10^{-10}$ W/in. Converting to the target coordinates, the alignment sensitivity is

$$\left|\frac{dP_1}{d\xi}\right| = \frac{l}{r}\left|\frac{dP_1}{dx}\right| \tag{22-46}$$

which for the center target is about 2×10^{-10} W/in. To detect a shift of 0.001 in. in the target requires a differentiation of

$$\left|\frac{dP_1}{d\xi}\right|\Delta\xi = (2 \times 10^{-10}) \times (10^{-3}) \text{ watts} \tag{22-47}$$

or 2×10^{-13} W for the middle target. The peak intensity, which is the energy striking the photomultiplier at the center of the image, is, from Eqs. (22-26) and (22-30),

$$I(0) = \left(\frac{A}{2l}\right)^2\left(\frac{256N^2}{\pi^4}\right)(2b)(2a) = \left(\frac{A}{2l}\right)^2 \frac{512N^2}{\pi^4}(Dw)^2 \text{ watts} \tag{22-48}$$

At the center of the accelerator, this is about 8.5×10^{-12} W.

Baffles

A baffle plate with a square opening has been mounted in the light pipe at each target position. The dimensions of the hole in each baffle were determined by the criteria that no light should get around a lens when it is inserted and that no direct rays from the laser should hit the inside surface of the pipe.

The combined diffraction pattern from all the baffles is very complex. It is actually such a diffraction pattern, not a spherical wave, which illuminates a lens. The alignment errors resulting from the baffles were calculated in Reference 2. The method used was to estimate the alignment error as a function of the asymmetry of the diffraction pattern from the baffles. The conclusion is that for any reasonable shift of the baffle, the resulting alignment error is negligible.

Vacuum requirements

The 24-in. light pipe must be evacuated to reduce the magnitude of refractive effects of the residual gas to below the alignment tolerance. Some care was taken during construction to avoid the introduction of heavy solvents or other chemicals with high indices of refraction, so that dry air will be assumed for the following calculations. A large oil diffusion pump with a refrigerated baffle is located at the laser end of the pipe, which has a volume of nearly 33,000 ft^3. The pumping system has proven capable of reducing the pressure to $\approx 10^{-2}$ torr in 8 hours. At this pressure, the system becomes conductance limited by the light pipe itself.

To calculate the effects of the residual gas, it is assumed that the index of refraction has the form

$$n(y) = n_0(1 - \varepsilon y) \tag{22-49}$$

where $n(y)$ is the index of refraction as a function of the vertical position y, and $n_0\,\varepsilon$ is the gradient of n in the vertical direction. The vector form of the differential equation of a light ray is[4]

$$\frac{d}{ds}\left(n\frac{d\mathbf{r}}{ds}\right) = \text{grad } n \tag{22-50}$$

Here $\mathbf{r} = \mathbf{i}x + \mathbf{j}y$, $\mathbf{i}$ and $\mathbf{j}$ are unit vectors, s is the distance along the ray, and y is the transverse coordinate; x is measured along the axis of the light pipe, and thus $s = x$ to a very good approximation. Substituting Eq. (22-49) on the right side of Eq. (22-50) gives

$$\frac{d}{dx}n\left(\mathbf{i} + \mathbf{j}\frac{dy}{dx}\right) = -\mathbf{j}\varepsilon n_0 \tag{22-51}$$

so that

$$\frac{d}{dx}\left(n\frac{dy}{dx}\right) \approx -\varepsilon n_0 \tag{22-52}$$

By integrating Eq. (22-52), it is found that if ε is small,

$$y \approx -\frac{\varepsilon x^2}{2} + Cx + C' \tag{22-53}$$

For a paraxial ray starting on the axis and parallel to it, both constants of integration are zero, and therefore,

$$y = -\frac{\varepsilon x^2}{2} \tag{22-54}$$

which gives the displacement of a light ray due to a gradient of the index of refraction in the light pipe. For the accelerator, the worst case is the middle target for which x is about 5000 ft. Hence, for an error of 0.001 in., which is the permissible tolerance, $\varepsilon \approx 5 \times 10^{-13}$ per inch.

To determine the gradient of the index of refraction, one may use the Lorentz-Lorenz formula in the form[5]

$$A = \frac{RT}{p}\frac{(n^2 - 1)}{3} \tag{22-55}$$

in which A is the molar refractivity, R is the gas constant, T is the temperature, and p is the pressure. Because n is very nearly unity, Eq. (22-55) can be written as

$$n - 1 = \frac{3Ap}{RT(n + 1)} \approx \left(\frac{3A}{2R}\right)\left(\frac{p}{T}\right) \tag{22-56}$$

to obtain the temperature and pressure dependence of $n - 1$. For dry air at standard temperature and pressure, $n - 1 = 3 \times 10^{-4}$. Thus, at any other temperature T and pressure p,

$$n - 1 = 3 \times 10^{-4} \frac{300^{\circ}\text{K}}{760 \text{ torr}} \left(\frac{p}{T}\right) = 1.2 \times 10^{-4} \left(\frac{p}{T}\right) \tag{22-57}$$

where p and T are measured in torr and degrees Kelvin, respectively.

To calculate the gradient of the index of refraction due to vertical temperature and pressure gradients, let

$$p = p_0 + p'y \tag{22-58}$$

and

$$T = T_0 + T'y \tag{22-59}$$

where p' and T' are the derivatives of pressure and temperature with respect to the coordinate y.

By substituting Eqs. (22-58) and (22-59) into Eq. (22-57) and expanding to terms of first order in y, one obtains

$$n - 1 = 1.2 \times 10^{-4} \left(\frac{p_0}{T_0} + \frac{p'y}{T_0} - \frac{p_0 T'y}{T_0^2} + \cdots\right) \tag{22-60}$$

Comparison of terms in Eq. (22-60) and Eq. (22-49) gives

$$n_0 \varepsilon = 1.2 \times 10^{-4} \left(\frac{p_0 T'}{T_0^2} - \frac{p'}{T_0}\right) \tag{22-61}$$

At 10^{-2} torr, $p' = -2.7 \times 10^{-8}$ torr/in. The pressure term then becomes $\varepsilon_p \approx 1 \times 10^{-14}$ per inch which is one-fiftieth of the tolerance derived above and can be neglected. The temperature gradient from top to bottom of the light pipe is not well known. Differences of about 0.1°C have been measured. Solving Eq. (22-61) for T' using the calculated tolerance for $n_0 \varepsilon$ yields

$$T' = \frac{n_0 \varepsilon T_0^2}{1.2 \times 10^{-4} p_0} = \frac{5 \times 10^{-13} \times (300)^2}{1.2 \times 10^{-4} \times 10^{-2}} \approx 0.037^{\circ}\text{C/in.} \tag{22-62}$$

which means that about 1°C differential is allowed from top to bottom of the 24-in. diameter light pipe. It is notable that the temperature term is the one that limits the maximum permissible pressure to stay within the tolerance for alignment.

Detector operation

The theoretical predictions of image size and detector sensitivity have been largely confirmed by experiment. The dimensions of the image patterns agree with the predictions of Eq. (22-43) except in the case of the targets

nearest the laser. For the target closest to the laser, it appears that the assumption of a point source is invalid. The image from the target is about 0.8 in. in diameter instead of the 0.4 in. calculated assuming a point light source. The magnification for this position is about 200, so that the center needs to be found only to within ± 0.2 in. to yield the required accuracy of locating the target. Actually, the sensitivity of determining the position of any target with the photoelectric scanner is ± 0.0001 in., which is the least count of the shaft encoder on the traverse system. The optimum aperture dimensions and scanning amplitudes which were calculated are only partially adhered to in practice. The scanning amplitude is adjusted according to the image width. However, the entire operation is done with a round aperture of 0.004 in. diameter. The photomultiplier has a sufficiently sensitive cathode that even this small aperture is enough to give a very adequate signal.

The detector assembly shown in Fig. 22-8 is mounted on the scanning system shown in Fig. 22-10. The arrangement of the observation equipment is shown in Fig. 22-11. By using the large swing mirror it is possible to divert the image pattern from the detector to a ground-glass screen.

Figure 22-10 Scanning assembly with the large mirror moved to the right to show the large vacuum window. Precision shaft encoders determine the position of the scanner to ± 0.0001 in.

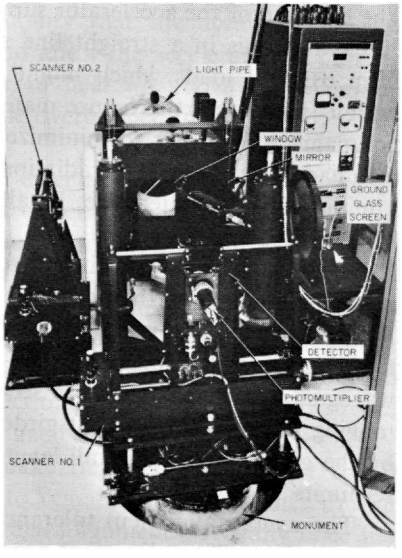

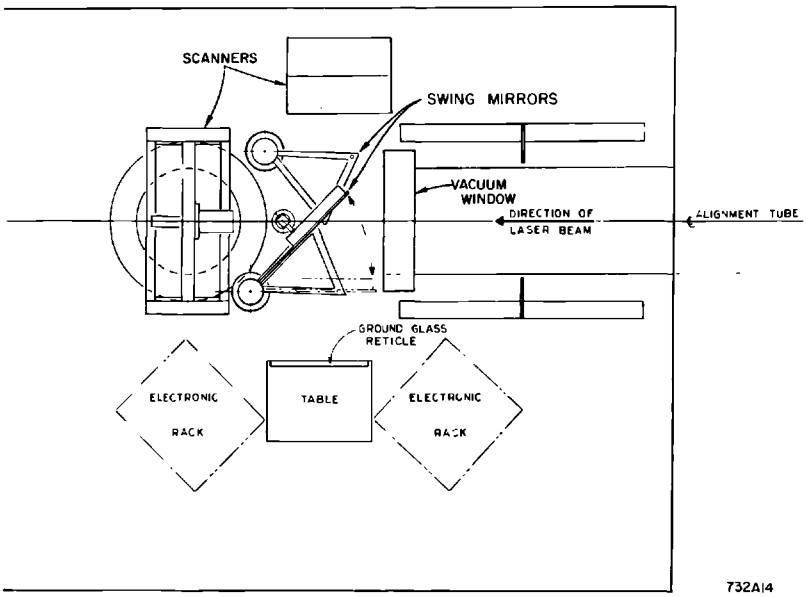

Figure 22-11 Layout of mirrors and observation equipment. By using a beam splitter, two coordinates of alignment can be monitored simultaneously.

22-2 The accelerator support system (DC, WBH, AVL, RCS, KS)

Design criteria

The function of the accelerator support system is twofold: to maintain the accelerator axis in a straight line and to protect the accelerating structure from external loads which might affect its dimensions and, therefore, its tuning. The support structure materials which are near the beam had to be nonmagnetic in order to minimize their interaction with beam optics, and they had to be resistant to radiation. The system had to be stable and require a minimum of maintenance. Finally, it had to have a minimum lifetime of 20 yr and be low in cost.

After initial alignment it had to be expected that the accelerator would move because of earth motions and that realignment would be required. Realignment causes relative motion between the accelerator sections and the klystron gallery. Such relative motion introduces reactions through the waveguides to the accelerator section. Because realignment is achieved by moving the ends of the 40-ft girders, adequate stiffness had to be provided by the girders over their full length to keep transverse deformations within set limits.

The overall alignment tolerance for the 2-mile length of the accelerator is ± 0.040 in. Thus alignment accuracy keeps the need for beam steering to

a minimum. Good alignment is especially important for multiple beams of different energies. The total laser system accuracy is ± 0.010 in., which left ± 0.030 in. for mechanical tolerances in the fabrication and assembly of supporting hardware in the disk-loaded waveguide, the 40-ft optical alignment system, and reading error. The ± 0.030 in. tolerance was allotted as follows. The accuracy of locating the optical tooling holes on the accelerator section at the lens end with respect to the center of the Fresnel lens mounting pins was ± 0.005 in. The tolerance for the location of the optical tooling holes with respect to the center of the accelerator mounting plate was ± 0.005 in. The straightness of an accelerator section mounted on its strongback was supposed to be within ± 0.010 in. Inaccuracies in the alignment tooling and reading error were given another ± 0.002 in. The remaining ± 0.008 in. was allowed as the tolerance for the deflection of the accelerator support structure under external loads.

In addition to the transverse alignment tolerance described above, there was also an axial location tolerance. This tolerance, which applies to the input end of each 10-ft section on a given girder, is ± 0.010 in. This location accuracy was achieved by mounting the input end of the first of the four accelerator sections rigidly to the 40-ft. girder. At this end, the girder is rigidly tied to the ground. The axial location of the successive three accelerator sections on each girder was fixed by spacers between sections.

During operation, the copper accelerator structure temperature is 113°F, whereas the supporting structure is at ambient temperature. Initially, the accelerator housing ambient temperature was approximately 55°F. As of July 1967, the housing temperature is approaching 100°F. Therefore, the support design had to permit a change in length of the supporting aluminum strongback while the accelerator section length remained fixed. Furthermore, it was necessary to recognize the possibility that the accelerator, water temperature, control system could fail and allow the accelerator sections to drop to tunnel ambient temperature or to heat up above the operating temperature to as high as 150°F before the overtemperature interlock would turn off the RF power.

While acting like hinges in the axial direction, the support assemblies had to be sufficiently stiff in the transverse directions to withstand side loads. Side loads could be transmitted to the accelerator sections through the rectangular waveguide in the event that the distance from the klystron to the accelerator changed. In addition to the external loads transmitted through the waveguide, transverse loads can be produced in any direction by an earthquake. The accelerating structure and its supports were designed to withstand an accelerating force in any direction equal in strength to the force of gravity. The structure also had to be designed so that its resonant frequency was outside of the predominant earthquake frequency range of 1 to 10 cycles/sec. The structure is not required to remain within tolerance during an earthquake but must return to its original alignment elastically once the earthquake load is removed.

Because of the radiation environment, the accelerator housing is relatively inaccessible. Thus, materials were chosen which exhibit long-term stability. For the same reason, the support system had to be designed in such a way that small alignment changes could be made quickly with minimum exposure to personnel. After this general discussion of design criteria, individual subsystems will now be described.

Twenty-four-inch light pipe

The 24-inch diameter light pipe serves the dual role of primary support girder for the accelerator and evacuated light pipe for the laser system. A round tube was the most rigid configuration obtainable for a given amount of material. The length of each girder module was determined by the requirement that it support four 10-ft accelerator sections fed with RF power by a common klystron. For the resulting length of 40 ft, a diameter of 2 ft gave the required stiffness. The wall thickness is $\frac{3}{8}$ in.

The girders were made by rolling aluminum plates and welding the longitudinal seam. After welding, each 40-ft segment of pipe was subjected to a fluoroscope inspection (optically magnified, visual x-ray technique). The aluminum pipe was then hydraulically expanded beyond its elastic limit into a 24-in. diameter cavity. This process brought the pipe to its finished form. The pipe dimensions were required to be within $+1/32$ and $-3/32$ in. on diameter, $\pm\frac{1}{4}$ in. on ovality, and straight to $\frac{1}{2}$ in. over the length of the pipe.

A 3-in. thick aluminum plate was used for the upstream end plate. It was called the target plate because it fixed the geometric relationship between the center of the accelerator sections and the center of the alignment target mounted to it. It also secures the pins of the intergirder connection hardware which supports the weight of the downstream end of the adjacent girder, and it provides for connecting the support jacks to the girder. Rather than to cut a full circle in the end flange to match the inside diameter of the pipe, a bridge was left to accommodate the target hinge. A flanged surface outside the pipe was provided for doweling the end plate of the first 10-ft accelerator section. These features are shown in Fig. 22-12. The 3-in. thick target housing was butt-welded directly against the upstream end of the support girder pipe.

The downstream end flange of the support girder pipe was made from a $1\frac{1}{2}$-in. thick aluminum plate. The plate was provided with a cutout hole slightly larger in diameter than the pipe so that it could be slipped over the 24-in. diameter and welded in position to yield the correct girder length to a tolerance of $\pm 1/16$ in.

Brackets for mounting the accelerator sections to the girder were welded to the 24-in. pipe. The accelerator support pads, when fitted with two vertical and one horizontal stud, permitted the alignment of the 10-ft accelerator sections relative to the target plate.

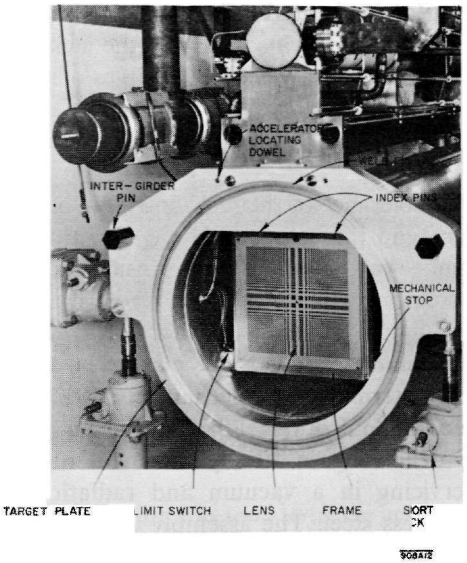

Figure 22-12 View of girder at target end.

The intergirder connection supports the downstream end of the girder. Adjustable rollers were mounted on the downstream end plate of each girder. A pair of hexagonal steel pins were fitted into conical holes in the target plate. The pins mate with the rollers and permit axial expansion of the girder. The joint also permits slight angular adjustments to be made between girders.

A 24-in. diameter aluminum bellows was welded between the adjacent ends of each pair of girders. The welding was done in place in the $2\frac{3}{4}$-in. wide gap between girders. The weld was made to a 1/16-in. thick fin which was left on the face of the end plates. A complete description of the girder fabrication method can be found in Reference 6.

Mechanical worm screw jacks serve as adjustable links between the support girder and the floor and wall of the accelerator housing. The wall jack permits making horizontal adjustments of the girder. This jack was braced to provide the longitudinal constraint. The floor jacks permit making vertical and leveling adjustments to the girder. In the bottom of each floor jack-strut, there is a system of springs that limits the maximum torque that any jack may introduce into the girder system. Ball rod ends connect the jacks to the girder and floor mounting bracket. The floor jacks are provided with a 6-in. adjustment permitting a readily available adjustability of ± 3 in.

To achieve the required axial stability, the wall jacks were provided with short 2-in. adjustment screws. The caps that guide the screw in the jack body were held to a maximum clearance of 0.003 in. Also, to reduce wobble to a tolerable minimum, it was necessary to build a bearing into the base of the jack body to support the jack screw.

For horizontal adjustments to the girder in excess of ± 1 in., 2 in. of shims were provided between the jack and its "A" frame support. They may be removed or added in multiples of $\frac{1}{2}$ in. as required.

Laser alignment hardware

The tolerance of the mechanical tie between the center of the laser alignment lens and the center of the accelerator section is 0.001 in. A spring-loaded hinge was mounted to the inside face of the target housing. A pneumatic actuator drives the hinge from outside the light pipe vacuum system through a vacuum tight mechanical connection. The Fresnel lens in its frame was pinned to the hinge plate. The "in" and "out" positions of the lens are determined by mechanical stops. Limit switches wired to lights in the remote control panel in the klystron gallery indicate the lens position.

The hinge assembly shown in Fig. 22-13, which must operate without servicing in a vacuum and radiation environment, was fabricated from stainless steel. The assembly consists of the lens mounting plate, the shaft, the constant force springs, and the mounting bracket. Constant force springs were attached to the hinge shaft to force the bottom edge of the lens frame against the mechanical stop. The torque is just sufficient to hold the frame firmly against the stop and to actuate the limit switch.

The hinge actuator shown in Fig. 22-14 consists of a pneumatically driven bellows assembly attached to a spring-loaded push rod. A bell crank hook is attached to the slotted end of the push rod. Both the bell crank and the spring cylinder are mounted on a common base bracket. The spring and the bellows work in opposition so that with the air pressure off, the spring retracts the target. As air is applied to the bellows, the pressure on the cylinder exceeds the force of the spring and allows the bell crank to rotate about its shaft and lower the target into the laser system. As the push rod extends forward, it does not apply any force to the bell crank; thus there is no external force on the target.

Figure 22-13 Target hinge.

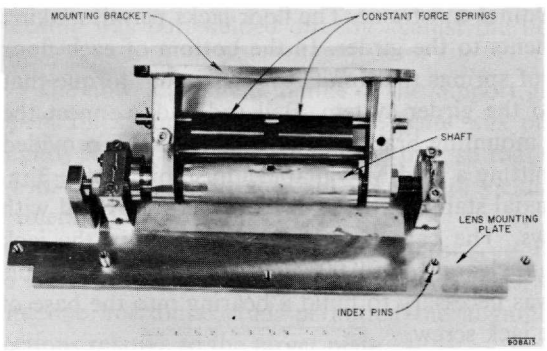

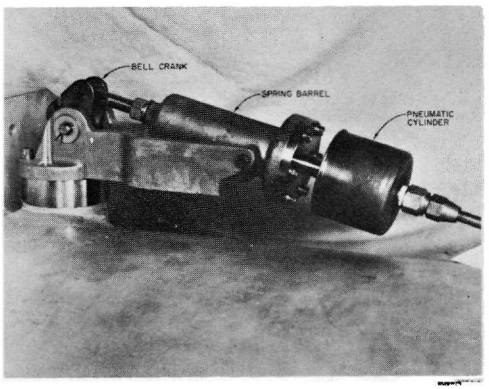

Figure 22-14 Hinge actuator.

A vacuum feedthrough with a universal motion was used to tie the actuator linkage to the hinge mechanism. This motion is achieved with a welded metal bellows arrangement and a rigid connecting rod which ties the hinge to the bell crank pin. The pin was threaded to permit adjustment. The vacuum feedthrough was fabricated of 300-series stainless steel plate and the bellows was made of precipitation-hardened stainless steel. The feedthrough is mounted on the light pipe on a boss welded to the pipe. The vacuum seal between the feedthrough and the light pipe is made by a metal gasket.

The position of the target is referenced by two limit switches. When the target is retracted, it makes contact with the upper switch attached to the hinge. When the target is inserted in the laser light path, the lower limit switch indicates that the target is in the correct vertical position. The switch wires were connected through an electrical feedthrough consisting of a connector sealed in a Pyrex–boro silicate glass insulation mounted in a Kovar flange. The flange was sealed to the light pipe by an indium wire seal.

Accelerator sections

The 4-in. diameter copper accelerator sections were fabricated in 10-ft lengths. The copper was fully annealed and, therefore, the sections could not support their own weight. Hence, immediately after fabrication, all 10 ft sections were permanently mounted on 10-ft aluminum extrusions, called "strongbacks." These extrusions and their mounts were designed to protect the accelerator sections and their input and output transition waveguides during processing and final installation. The mounts were designed to permit differential thermal expansion between the aluminum supporting structures and the accelerator sections. Four of these 10-ft accelerator sections were mounted and aligned on each 40-ft aluminum support girder as shown in Fig. 22-15.

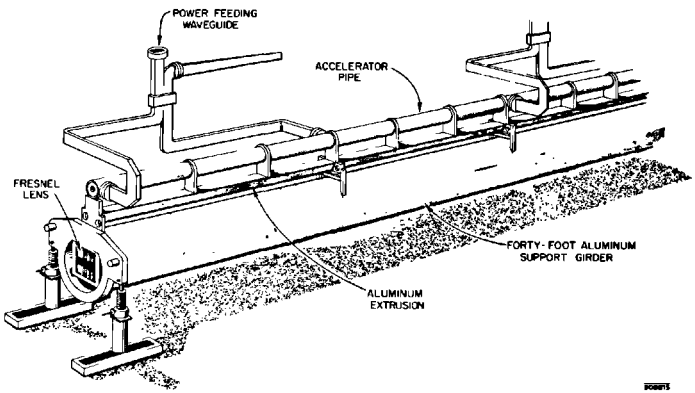

Figure 22-15 Sketch of 40-ft girder.

The specific design criteria placed on the accelerator section support structure were

1. With the accelerator section displaced along its axis by 0.275 in. relative to the strongback and under operating conditions, no combination of the loads shown in Fig. 22-16 should cause a total transverse displacement greater than ± 0.010 in. vertically, ± 0.008 in. horizontally, or a twist greater than 0.2 mradian. (See Fig. 22-17).
2. With the accelerator section displaced along its axis by 0.375 in. relative to the strongback during transportation or other temporary condition, no combination of the loads shown on Fig. 22-16 should cause total transverse displacements exceeding twice the maximum displacements listed in (1) above.
3. The maximum axial force in an accelerator section from all supports used on one 40-ft girder should not exceed 750 lb during accelerator operating conditions.

Figure 22-16 Design loads and axial displacements at the free downstream end of the 40-ft girder.

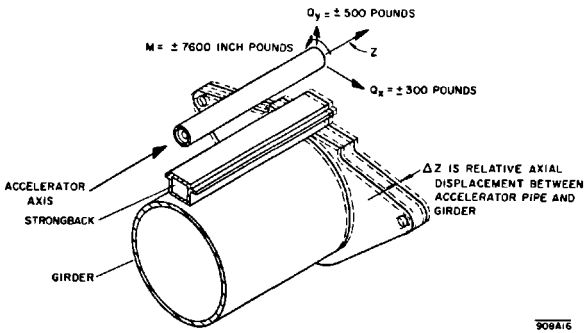

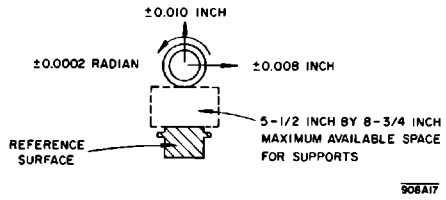

Figure 22-17 Allowable transverse displacements at the downstream end of the 40-ft girder.

4. The supports should be capable of withstanding shock loads of 2 times the design load without permanent deformation.
5. After the supports have been cyled axially 600 times with full design load, between plus and minus 0.372 in., they should still meet criteria (1), (2), (3), and (4).
6. The supports should require no maintenance.
7. The support assembly should be made from nonmagnetic materials.
8. The supports should be of a frictionless and elastic type such that, when all external loads on the accelerator sections are brought back to their original values, the accelerator sections are also restored to their original position.
9. Each 10-ft assembly should provide accurate and easily accessible references for alignment of the accelerator sections on the 40-ft girder.

All the 10-ft support structures were built from assemblies as shown on Fig. 22-18. Interchangeable subassemblies were used to build the support

Figure 22-18 Ten-foot accelerator section mounted on aluminum strongback.

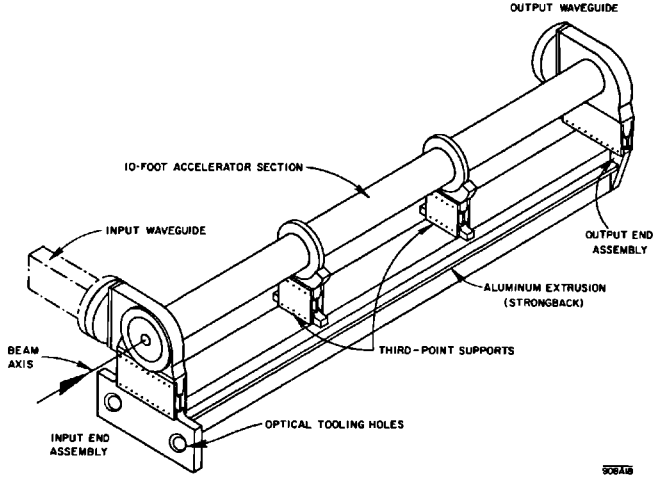

structures for ease of manufacture and cost saving. A typical support structure was made from an aluminum extrusion, an input-end assembly, an output-end assembly, and a pair of one-third point supports.

The input- and output-end assemblies were essentially identical except that only the input-end assembly had optical tooling holes. The optical tooling holes and the locating hole for the disk-loaded waveguide were machined into the end assemblies in a triangular pattern having an 11-in. base line and 10-in. height to a dimensional accuracy of ± 0.001 in. The optical tooling holes were later used in the alignment of the 10-ft assemblies on the 40-ft girders and also in the alignment between girders. Lateral and axial alignment of the downbeam end of each 10-ft section was achieved by the use of stainless-steel locating and spacing rings. These rings aligned one accelerator section with respect to another by mating with concentrically machined recesses at the ends of the accelerator sections.

The first input-end assembly used on each girder was bolted rigidly to the girder target housing. The rigid end assembly was made by using a larger mounting plate and eliminating the flexible section. The last accelerator section on each girder had mounting plates with tooling holes at both the upbeam and downbeam ends. The optical tooling holes of the downbeam end were used to align the accelerator section on the girder and then to make the intergirder cross-joint alignment. Six different end assemblies were produced, all capable of being mounted at either end of the aluminum extrusions. Different combinations of these subassemblies were then used to produce all the required support structures.

Figure 22-19 Flexible support assembly (cross section to scale).

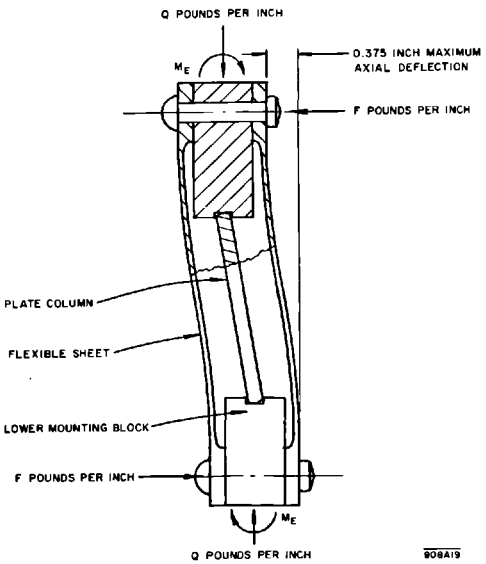

Most of the support subassemblies included a flexible section built as shown in Fig. 22-19. This riveted part of the subassemblies consisted of two flexible aluminum sheets, an upper and a lower mounting block, and a spring-tempered, phosphor, bronze plate column. The plate column, which was rounded at both ends, was inserted with a compressive preload to insure that an external tensile load would not cause separation between the plate column and the mounting blocks. The flexible assemblies carried the weight of the accelerator sections plus any external loads while deflected axially as shown in Fig. 22-19. During this deflection, the plate column rolls on its ends and the sheets bend. This design was chosen since it was capable of providing very high lateral stiffness and almost any chosen axial stiffness.

The 10-ft aluminum extrusion provides support for the 10-ft accelerator section at the one-third and two-third points as well as at the ends. The extrusions are never exposed to external loads, all external loads being carried through the end assemblies directly to the support girder. The aluminum extrusion was designed to limit lateral deflections of the accelerator sections to 0.030 in., when exposed to accelerations of $\sqrt{2}\,g$ in any direction.

The aluminum extrusion was a 10-ft long box beam. A lip on each side was provided for mounting of the third-point supports.

The assembly of the accelerator section to the support structure was performed on a granite block which had special built-in tooling. The accelerator sections were mounted on the preassembled support structures, and the third-point supports were adjusted to bring these two points on the accelerator section in line with the ends to within 0.002 in. For a more complete description of the accelerator support assemblies, see Reference 7.

Drift sections

Drift sections are located at the end of every sector along the two-mile linear accelerator. The drift sections are used for beam guidance and diagnostic purposes. (See Chapter 15 for a more complete description of drift section components.) A typical drift section is shown in Fig. 5-22. Each component is mounted on the strongback by means of support plates which contain optical tooling holes. The support plate position is adjustable for alignment. The entire assembly is approximately 9 ft long and weighs 630 lb. The drift tubes at either end of the drift section contain bellows through which the assembly is connected to the accelerator vacuum system. A manual thin valve at the upbeam end and an automatic thin valve at the downbeam end allow the drift section to be isolated from the remainder of the machine vacuum. A description of the thin valves, their function and operation, is contained in Chapter 23. The drift section assembly is supported by a special 10-ft length of the 24-in. light pipe.

The alignment tolerances of the various components with respect to a theoretical beam axis were: quadrupoles, ± 0.005 in.; beam position monitor assembly, ± 0.024 in.; beam intensity monitor, ± 0.062 in.; steering

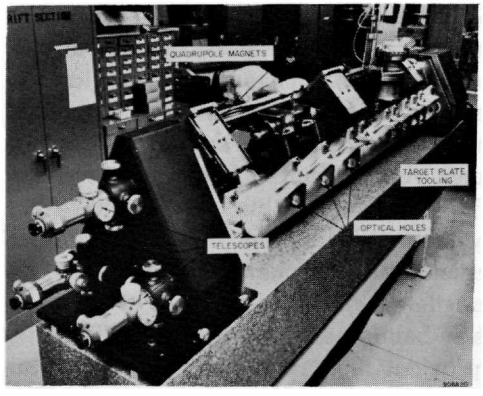

Figure 22-20 Drift section alignment.

dipole, ± 0.030 in.; and beam profile monitor chamber, ± 0.035 in. The beam scraper alignment tolerance with respect to the following accelerator section was ± 0.010 in.

Before installation, the positions of the optical tooling holes in the support plates were fixed relative to the center line of the components. The support plates were, in turn, attached to the strongback by adjusting bolts.

The final alignment was made after all the components were mounted on the strongback so that the strongback was supporting the full weight (510 lb) of the components and had undergone its full deflection. The alignment was carried out on a three-telescope station shown in Fig. 22-20. The telescopes were mounted at the vertices of a triangle having an 11-in. base line and a height of 10 in. The telescope positions were adjusted for translation and angulation within the telescope mounting structure. The telescopes were aligned relative to a pair of special target plates which were mounted at the ends of the drift section. The target mounting plates were made of the same aluminum alloy as the component support plates and the strongback. Each plate held three see-through wire targets in the 11×10 in. triangular pattern. The target holes in the pair of target plates were jig bored together in one operation.

The drift sections were designed to be readily replaceable in the event of failure of a component, and spare full assemblies are being maintained. This approach was chosen because a complete drift section assembly can be replaced more quickly than an individual component. Mounting plates which have supporting surfaces accurately located with respect to optical tooling holes were mounted on each end of a drift section support girder. The support plates were located with respect to the Fresnel lens in the standard fashion described earlier in this chapter.

The optical tooling holes on the magnetic quadrupole lenses were located with respect to the mechanical center of the aperture. The mechanical center

was found by using a self-centering target. Initially, the center of the quadrupoles was determined by inserting a vial containing a colloidal ferrite suspension into the space between pole pieces. The magnet was then energized, and the pattern formed by the colloid[8] was observed. For the initial drift section installation, which contained quadrupole triplets rather than doublets, the quadrupoles were aligned using the colloidal suspension. The drift sections which were removed from the accelerator and reworked to contain quadrupole doublets were aligned mechanically. To within the accuracy of either method (± 0.001 in.), one could not discern a difference between the results of using the colloidal suspension and the results of using a self-centering target.

The beam position monitor assembly is described in Chapter 15. The center line of the position monitor was located by reference to external surfaces which were machined accurately to be concentric with the aperture between cavities. The structure is held by support plates which again have optical tooling target holes.

The alignment tolerance for the steering dipoles was sufficiently loose and the configuration was such that they could be aligned with respect to the drift tube. The dipole supports, therefore, have no optical tooling holes.

The beam profile monitor chamber was designed to house any special beam monitoring equipment which might be required. Seven of them contain profile monitors. The large flange to which equipment housed in the chamber is bolted serves as the reference surface to which that equipment is aligned. The equipment is thereby located accurately with respect to the optical tooling holes in the support plates. The support plates are bolted and doweled in place. The profile monitor chambers in Sectors 5, 13, 21, and 29 have been replaced by pairs of orthogonally mounted C-band waveguide cavities for detecting transverse beam oscillations associated with the beam breakup phenomenon (see Chapter 7).

The beam scraper serves as a fixed protection collimator for the accelerator sections in the sector following the drift section. The scraper bore is 0.673 in. and its effective length is 22 radiation lengths. The smallest aperture in the accelerator section is 0.7517 in., so that the scraper offers good protection against diffuse beams which tend to fill the aperture as well as against misteered beams. The beam scrapers are water-cooled. The support points on the beam scraper o.d. are machined to be concentric with the i.d. of the scraper. The support plates are similar to those used for the beam position monitor assembly.

Monument target system

Monument target girders are located at three places along the accelerator. In addition to their normal function, these girders contain special Fresnel lenses which are mounted to concrete monuments. The monuments are independent of the accelerator housing and extend through the floor of the

housing into the bedrock layer. The four monument lenses are used to observe changes in accelerator alignment relative to the underlying rock. Special girders were fabricated with box sections to house the monument lens and its support structure.

A pair of bellows makes a flexible vacuum connection between the girder and a shaft that runs through the length of the box and supports the lens. The shaft is fixed relative to the concrete monument. The hardware that supports the lens on the shaft is statically balanced so that there is no tendency for the shaft to rotate as the lens is swung in and out of the laser beam on its vertical axis. Outside the bellows, the shaft is positioned relative to the monument on an adjustable support system. This support fixes only the horizontal, vertical, and axial position of the shaft. The shaft is free to rotate on roller bearings in this support. Rotations of the girder relative to the monument, therefore, do not strain the support hardware, but the girder must be level for the position to be correct.

Fixtures were supplied at the time of assembly to maintain the proper target position relative to the girder. When the girders were installed, the connection to the monument was made and the support fixtures were removed. This arrangement is shown in Fig. 22-21.

Each monument girder is provided with a 24-in. diameter access port to permit servicing the monument target hardware. On occasion, these ports have served the additional purpose of providing access for a lean and agile technician to do maintenance inside the girders, as far as 500 ft away.

Figure 22-21
Monument target support.

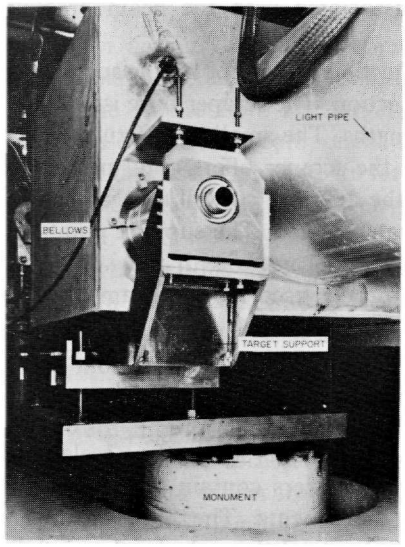

Positron source girders

The positron source station occupies a length of approximately 40 ft in Sector 11 and contains both standard and special beam-monitoring equipment, steering dipoles, focusing solenoids, a pulse deflection magnet, an RF deflector, accelerator sections, in-line thin vacuum valves, and the positron radiator itself. The design of the source and the function of these components is described in Chapter 16. The total positron station weight is approximately 16,000 lb as compared to 4000 lb for a standard girder. To accommodate this weight, the components were distributed among three shorter girders. The first positron girder is 10 ft long and supports 6500 lb. The second girder is also 10 ft long and supports 4000 lb. The third girder is 20 ft long and supports 5500 lb.

The positron wheel source and its drive mechanisms are supported from the floor of the accelerator housing and aligned with respect to the beam axis by means of fiducials placed on the wheel support structure. Any realignment of the first positron source girder requires a realignment of the wheel radiator. The wand radiator source is mounted to a 6-in. flange on the back of the radiator housing and is supported directly from the housing. The alignment of the wand is, therefore, independent of any girder alignment. The initial alignment of both positron source radiators was made by removing the drift tube ahead of the positron source and sighting down the beam line at the inserted target.

A strongback is used to support the positron source components in order to make the installation and removal process for the positron source as fast as possible. The rapidity with which the radiator strongback can be removed is very important because of the high radiation levels in this area. The mounting method is similar to that used for the drift sections. Special equipment must be used for handling the positron source because of its weight. Carriages and hoists traveling on overhead rails are used for handling the source. Additional permanently installed handling equipment is used for removal of either of the source radiators.

The two accelerator sections following the positron source are supported by concentric strongbacks which fit into the solenoid coils. The strongback consists of an 8-in. diameter nonmagnetic stainless steel pipe to which the accelerator section is rigidly attached at the upbeam end. Sliding supports keep the accelerator section straight while allowing it to expand axially with respect to the strongback and the girder. Holes were provided through the wall of the strongback for tuning the accelerator section after it was mounted in the strongback and for measuring the straightness of the accelerator section within the strongback. Alignment of the accelerator section is made by reference to special optical tooling plates which are clamped to each end of the accelerator section.

The solenoid coils are supported by box-like frames. The frames have optical tooling plates on each end. The coils were first mounted on the frames

and rough-aligned mechanically. The coils were then energized and their magnetic center determined. The coil positions on the frame were adjusted to make the magnetic center coincident with the accelerator axis.

Injector girder

The main injector girder is 30 ft long. It supports the gun, parts of the gun modulator, ion pumps, the prebuncher and buncher, an accelerator section, solenoid coils, beam position and intensity monitors, and the beam knockout. A complete description of the injection system can be found in Chapter 8. The accelerator section is mounted in a nonmagnetic stainless steel concentric strongback. The strongback is sufficiently stiff to support both the weight of the accelerator section and the solenoid coils. The accelerator section is rigidly attached to the strongback at the upbeam end and is allowed to slide downbeam within the strongback to permit thermal expansion. The strongback is, in turn, rigidly anchored to the girder at the upbeam end and is supported by flexible supports at its midpoint and downbeam end. The accelerator strongback has a series of holes opposite each cavity so that the accelerator section can be tuned after insertion into the strongback. Additional holes allow for measuring from the strongback o.d. to the accelerator section for centering it inside the strongback. Optical tooling holes are incorporated into the accelerator supports. The components downbeam of the accelerator section are mounted on a strongback similar to that used for the drift sections.

Beam-analyzing stations

The two beam-analyzing stations (BAS) described in Chapter 15 are located in the accelerator housing. BAS-1 is located just downbeam of the injector on girder 1-1; BAS-2 is located on girder 20-1.

Figure 22-22 Beam-analyzing station (BAS-2).

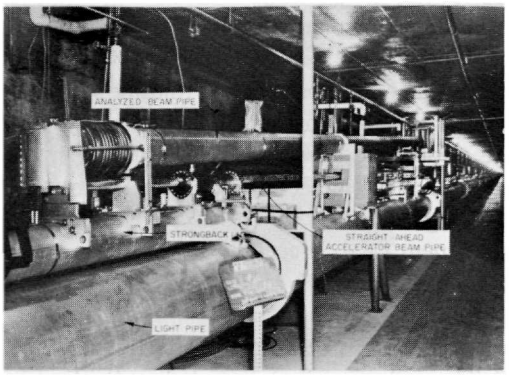

The BAS-1 is approximately 10 ft long and replaces the fourth accelerator section on girder 1-1. It is shown in Fig. 15-16.

The beam-analyzing station at Sector 20 (BAS-2) can be seen in Fig. 22-22.

On both beam-analyzing stations, the components which had to be aligned accurately were mounted on a strongback similar to the drift section strongback and aligned prior to installation on the girder. A three-telescope station was used to align the magnets with respect to the optical tooling holes on the strongback. The deflection magnet pole pieces were aligned parallel to the beam axis and centered on the axis by measuring an offset from one of the pole faces. The magnet angle was set by means of a sine bar and level. Magnet rotation about the beam axis was set using a level.

Quadrupole singlets

Quadrupole singlets were installed at 40-ft intervals in Sectors 1 through 6 as discussed in Chapter 7. They are located between 40-ft girder assemblies, around a drift tube and bellows assembly which joins two girders on the beam line, as shown in Fig. 22-23.

The quadrupoles were attached to a supporting bracket which had two clearance holes at the location of the optical tooling hole. Adjusting screws on the bottom and side of the clearance holes allowed the optical tooling target to be positioned within that hole. After the support bracket was attached to the quadrupole, the assembly was mounted on the drift section

Figure 22-23 Quadrupole singlet installed between two 40-ft girders (Sectors 1 to 6).

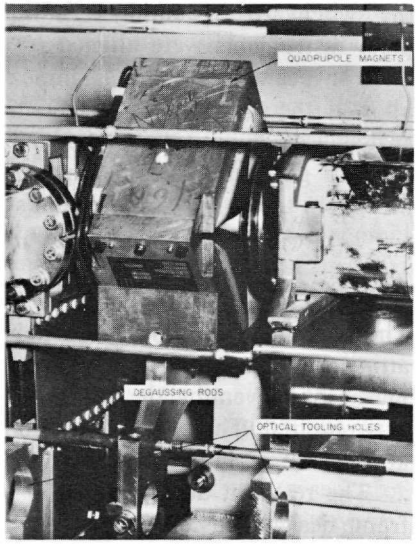

alignment and assembly station which contains the three-telescope stand. The magnet was adjusted until its center lay on the upper optical alignment sight. The magnet was also leveled and adjusted for pitch, roll, and yaw. The target positions were then adjusted to coincide with the two lower lines of sight and the adjusting screws locked in place. The equipment used for this activity was the same as that described previously for the quadrupole alignment in the drift sections. At installation, the quadrupole magnets were disassembled, slipped under the drift tube and bellows assembly, reassembled, and mounted to the target housing plate at the upbeam end of the girder.

The 40-ft quadrupoles were aligned at installation by a mechanical centering alignment tool consisting of an arbor centered on the end-plate target holes by means of centering plugs. A gib in the arbor was tapered 0.005 in./in. Sliding the gib axially changed the radial distance from the arbor center line to the surface of the gib. Calibration marks were placed on the gib to indicate dead center (0.750-in. radius) as well as ± 0.002-in. displacements. The magnet position was adjusted until the optical tooling holes in the magnet support plates were in line with the target holes on the adjacent accelerator support plates. This condition was indicated when the gib just touched the screws in the optical tooling holes. The alignment was carried out on one side of the accelerator. The other side is aligned by using a transverse level going from the wall side target across to the arbor shaft.

Beam switchyard support girders

The final four light pipe girders of the accelerator constitute the beginning of the BSY instrument section. The girders were specifically designed to support the instruments in the same manner as they are supported throughout the switchyard. Mounting rails were welded to the o.d. of the aluminum pipe. Instruments were aligned to the correct position with respect to the electron beam axis by an alignment fixture referenced from the rails. This allowed the diagnostic instruments to be interchangeable throughout the switchyard. A cryogenic differential vacuum baffle is mounted on one of the BSY girders. This baffle separates the high vacuum system of the accelerator from the switchyard vacuum system.

Light pipe vacuum restraints

The vacuum within the 24-in. light pipe creates an external force due to atmospheric pressure of approximately 6500 lb axially along the pipe. A means of preventing the collapse of the intergirder bellows under vacuum was required. Therefore, restraints were attached to the light pipe sections at the extreme ends of the accelerator.

The restraint at the upstream end of the accelerator is of a fixed "A" frame design. This "A" frame is adjacent to one of the accelerator alignment reference points, so that no adjustment features are required.

At the downstream end of the accelerator, the vacuum restraint is designed to permit vertical and horizontal adjustments as required for accelerator realignment. To make this hardware adjustable, rollers similar to those in the pin and roller bearing assemblies were used to permit vertical and horizontal motions with minimum resistance as the floor and wall jacks adjacent to the restraint are adjusted.

In an attempt to eliminate any possibility of failure of the two restraints, a safety factor of approximately 10 was used in the design of the structures and in the method of attaching them to the floor of the accelerator housing.

Installation and initial alignment

The 40-ft modules of the accelerator were assembled on stands as shown in Fig. 6-40. Four accelerator sections were mounted to each module of the light pipe. The alignment operation was performed using the telescopes visible at the near end of the pipe in Fig. 6-41. The first step consisted of positioning the nearest section as accurately as possible relative to the support plate to which the Fresnel lens is fastened. The second step consisted of adjusting the positioning screws for the end supports until the four accelerator sections were aligned along a line parallel to the axis of the light pipe.

Several difficulties were encountered in the above operation which are worth reporting. First, the hinge assemblies which support the Fresnel lenses were found to be sensitive to the force required to insert them. The hinges were modified after about 20% of the installation was complete, but this meant that in those cases in which the hinge had to be replaced by a modified model, the initial position of the lens was lost.

Next, it was found that temperature stability in the assembly area was not good enough to permit accurate adjustment of the position of the four accelerator sections on each girder. There are always difficulties in using optical tooling techniques over distances of more than a few meters. This is particularly true of a system which has not come to temperature equilibrium. Refractive effects due to temperature gradients in the air limited the observations to accuracies of from 0.01 to 0.04 in.

There were also doubts, which turned out to be well founded, that the alignment within each module would remain correct after the assembly was moved to the accelerator housing and installed. Installation included connecting the rectangular waveguides which could put some vertical loading on the girder.

Several times during the assembly process, there were difficulties with the tooling jigs, which were not found until after the module had been installed. The problems involved in returning these modules to the assembly line were such that in almost all cases the rework was done in the field.

The net result of these and other lesser problems was that a series of setups had to be devised to permit repeating effectively all these operations on the installed accelerator. The largest effort was to determine the

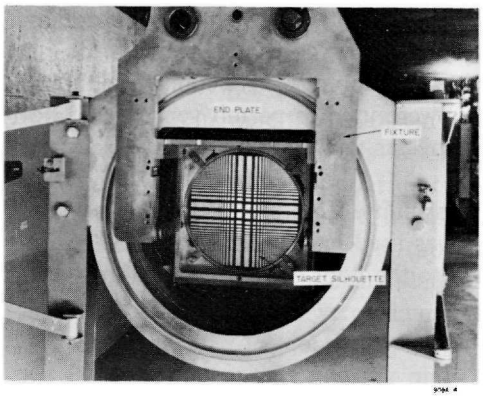

Figure 22-24 Calibration jig being installed on a special calibration girder.

displacement of the accelerator relative to the Fresnel target. A ruled ground-glass reticule plate was suspended in a jig from the optical tooling holes at the end of an accelerator segment. Figure 22-24 shows the jig fixture being installed on a special test and calibration girder. The glass was positioned as close as possible to the target. A light was projected from the other end of the module against the face of the target. The silhouette of the target thus appeared on the glass plate with the rulings superimposed. A set of five photographs was made of each target with a 35-mm camera and a one-to-one closeup lens. A sample of the one-to-one photography is shown enlarged in Fig. 22-25. On the accelerator, the entire operation had to be performed by working through a $2\frac{3}{4}$-in. slot between girders. The vacuum bellows were welded in the gap as soon as the photographs were checked. From the first

Figure 22-25 Photograph used to calibrate position of installed Fresnel target.

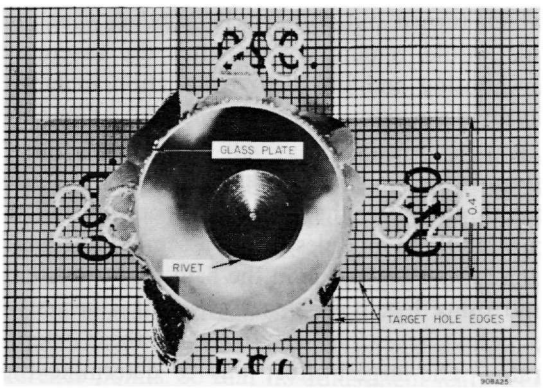

checks with this photographic calibration, it was apparent that the accuracy with which the targets were located on the accelerator was not as good as expected. This meant that it was necessary to carry out the photography on every one of the 272 girders. Counting calibration shots and retakes, about 600 sets of pictures were made. The displacements of the target slot edges from the reticule lines were read on a micrometer microscope. Twelve edge readings were made in both the horizontal and vertical directions for each target. The data were analyzed by computer with a program which checked that the data were consistent within themselves and with the target that was supposed to be installed at that location. It is estimated that the accuracy of determining the target position was about 0.005 in. Repeatability was about ± 0.002 in. No satisfactory explanation was ever found for the failure of the original telescope system to yield consistent results. Errors of ± 0.020 in. were common for a method which should have been 20 times better.

The accelerator was initially installed along a line determined by conventional surveying. Figure 22-26 shows the observed results when the laser system was first activated. Although the spread in vertical and horizontal alignment was about the same, it is possible to see a pattern in the horizontal alignment while the vertical spread appears random. The pattern in the horizontal alignment was probably due to errors in locating secondary reference points by sightings from the surveying towers at the ends of the site. The actual placement of girders was made over marks made from these

Figure 22-26 Accuracy of initial alignment as measured by laser system. Initial alignment was accomplished using conventional surveying techniques.

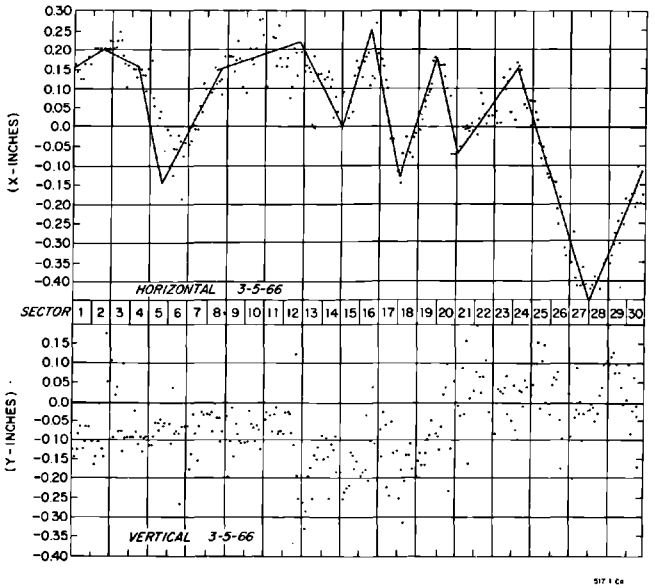

secondary points. The vertical survey used local gravity as a reference and, thus, was probably better. However, the placement of girders vertically was done with less precision.

The process of aligning the accelerator with the laser system required that a two-man team work along the accelerator while in communication with an operator in the alignment observation room. The alignment of the accelerator was dependent on keeping the support girder level in the transverse direction. A precision bubble level was placed between the optical tooling holes so that the differential extension of the two floor jacks could be equalized. The alignment procedure was as follows. The operator in the observation room observed and recorded the position of the laser image. By referring to a table of coordinates, he then set his detector to the correct position and instructed the team to adjust the position of the girder until the detector read a null signal. When the girder was set in both translation and elevation, the level was rechecked. The procedure required about 15 min per station and was accurate to 0.001 in. A record of how far the girder was moved was obtained by using the initial readings in a computer program to determine the alignment error at the point in question. The amount moved was recorded and was equal and opposite to the calculated error.

The alignment results from the first use of the system were checked by stretching a wire through the tooling holes on successive sets of three girders. Thus, if a gross error was made in determining the correction factor on the location of one target, it showed up in a displacement of that girder relative to its neighbors. The wire was observed both vertically and horizontally by a system based on detecting the magnetic field from a 1000-Hz current which was passed through the wire. Modified stereo tape recorder heads were

Figure 22-27 Stretched wire pickups.

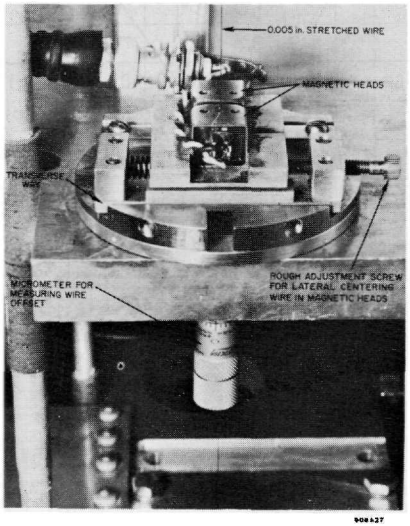

used as pickups for the alternating magnetic field. When the signal was exactly balanced between opposite heads, the discriminator read a null signal. Figure 22-27 shows the detector assembly with the micrometer screws used to position the heads. The head fits into an optical tooling hole. By means of a cam wheel, the head is expanded until it is centered in the hole. The total span of the wire was from 60 to 100 ft. The wire was tensioned by a weight over a pulley. A sufficiently high tension was used so that the catenary sag was of the order of 0.040 in.

The four accelerator sections on each segment were realigned after all the above operations had been completed. By this time, the accelerator was at its normal operating temperature of 113°F, and all waveguides, vacuum manifolds, and water lines were connected. The forces from these loads cause some sag in the girder. This alignment operation could have been done best by the stretched wire method but it was faster to use a pair of conventional alignment telescopes, one on each side of the girder. The telescopes were mounted in the optical tooling holes at the Fresnel lens end of a girder and were bucked into sighting targets in the corresponding holes in the next girder. The targets were then inserted, one at a time, on each side in the holes on each section and indicated adjustments were made.

Figure 22-28a Accumulated horizontal alignment changes, 1 yr after installation.

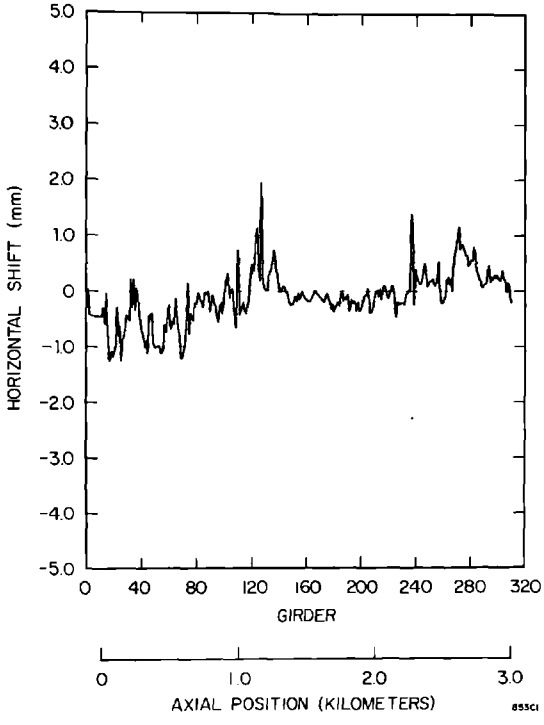

Stability

Information about long-term stability was obtained by referring to four monuments which are located along the accelerator. Three of the monuments have Fresnel lenses mounted as described earlier. The fourth monument was used as the base for the detector. Alignment data taken at any time can be calculated with reference to the straight line determined by any two points along the accelerator. Whenever a pair of the monuments are chosen for this purpose, the results give the total shift since the initial alignment.

The results of the operation of the alignment system for the first year are shown in Figs. 22-28a and b. The changes shown are accumulations of changes which were corrected by periodic realignment. The largest settlements occurred in areas constructed over filled ground. The correspondence between settlement and fill is quite striking. The implication is that those parts of the accelerator which were built directly on subsurface rock are quite stable. Fortunately, the more critical areas of the BSY and the end stations are all built directly on the underlying sandstone.

Figure 22-28b Accumulated vertical alignment changes, 1 yr after installation.

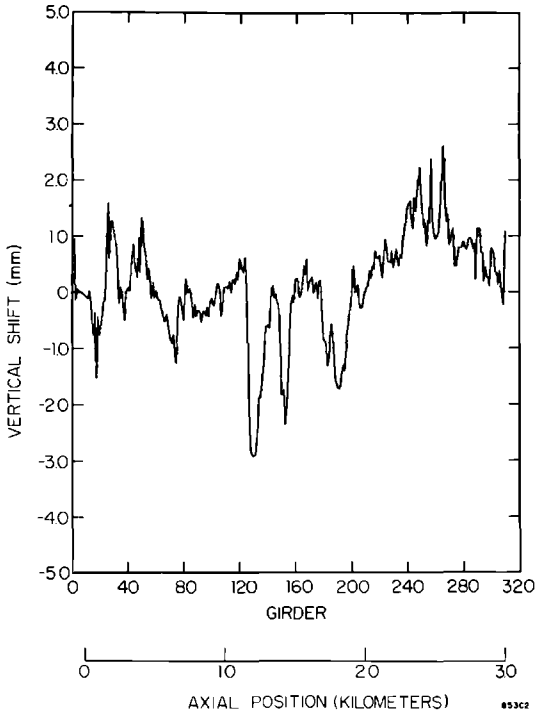

22-3 The beam switchyard support and alignment system (DC, WBH, JKW, JGN)

Summary of requirements

The support and alignment of the BSY is described in this section. It will be recalled from earlier chapters that the purpose of the BSY is to deliver the electron beam from the accelerator to the experimental areas. The switchyard consists of an elaborate system of bending magnets, magnetic quadrupole lenses, protection devices, and diagnostic instruments. These elements are primarily divided among two transport systems* leading to the experimental areas. (See Fig. 17-1.) The two systems, labeled A and B, after the experimental areas they serve, have a common origin in the beam line from the accelerator. A list of the most pertinent design parameters of these two systems is contained in Table 17-2.[9,10] The problems of support and alignment are primarily those of meeting the requirements set forth in this table.

The following procedures were used to insure the utmost accuracy in the alignment and placement of components in the BSY. An extension of the accelerator laser alignment system was used as a primary reference line. Secondary reference points from which measurements could be made were established along the path of each beam by using stretched wires and accurately scribed tapes. The distances between components or between a component and a reference point were set by tapes scribed with the proper distance. A tape bench facility was built for scribing these tapes. When properly installed, most components in the switchyard are tilted. A special optical alignment shop was established for measuring the angles of tilt and for targeting the components to insure proper installation. Finally, the angles and distances required for the correct alignment of components were calculated, taking into account the effect of the curvature of the earth upon these parameters.

The basic optics of transport system A is shown schematically in Fig. 22-29. System B is very similar. Each system lies in a distinct plane (see Fig. 22-30). The exit beam lines are required to be horizontal with respect to local gravity in the experimental areas. The accelerator axis points downward by 4.74 mradians with respect to the local gravity vector at the beginning of the switchyard. The respective exit beam lines for the A and B systems and the common accelerator line define the two planes in which the beams lie. A major part of the alignment effort involves targeting each component so that it can be aligned in its respective tilted plane while a local gravity reference can still be used for making measurements.

The tolerances reported in Reference 9 were calculated using the error analysis features of the TRANSPORT computer program.[11] The criteria

* As this book is being written a third system leading to experimental area C is being installed straight ahead.

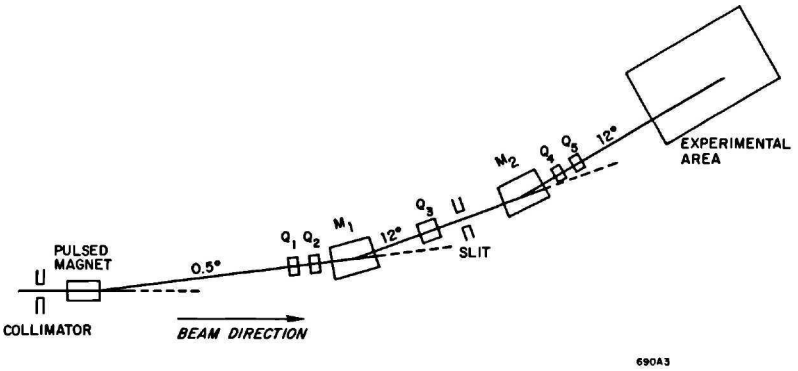

Figure 22-29 Schematic diagram of an achromatic bending system (transport system A) in the BSY.

that place the strongest limitations on the position tolerances are energy resolution (see Table 17-2) and the apertures of the switchyard elements downstream of the element being aligned.[12] The most restrictive translation alignment tolerance applies to the horizontal and vertical positions of either element of the first quadrupole doublet (see Table 17-3). This tolerance is based on the fact that a translated quadrupole is equivalent to a quadrupole plus a dipole. The most restrictive rotational alignment tolerance is ± 0.33 mradian for rotation about the beam line axis for magnets in the first bending group, M_1. This rotational tolerance is necessary to constrain the vertical component of the bend. Although many of the other tolerances are less restrictive, some of them are as difficult to achieve. For example, the switchyard is about 1000 ft long and a longitudinal tolerance of only 0.01 ft represents an alignment precision of 1 part in 10^5.

Figure 22-30 Tilted planes of A- and B-beams in the BSY.

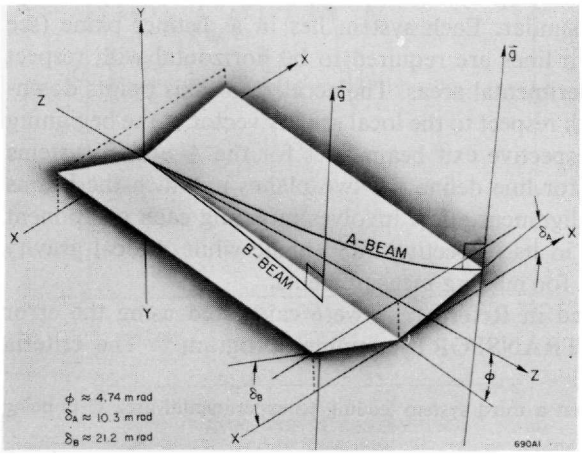

Laser reference line

An extension of the accelerator laser alignment system (see Section 22-1) provides a reference line throughout the first half of the switchyard. The function of this extension is to locate alignment targets with transverse coordinates to within ± 0.002 in. These target positions are then used as references for positioning the components in the beam lines. Figure 22-31 shows a laser alignment target stand and a portion of the vacuum pipe through which the laser beam travels.

The extension has a separate laser located at the east end of a 10-in. diameter vacuum pipe which extends approximately 750 ft beyond the end of the accelerator. It includes twenty alignment positions, each of which has a retractable Fresnel lens, the position of which can be determined by the operator in the Alignment Room at the beam injection (west) end of the accelerator. The Fresnel lenses are similar to the targets in the accelerator system but they are smaller (up to 6×6 in.). The 10-in. switchyard pipe is tangential to the bottom of the 24-in. accelerator pipe at the coupling point. The reduction was required because of the size of the collimators (see Fig. 5-24 and Chapter 20) which prevented use of a 24-in. light pipe throughout the switchyard. In view of the fact that the reference line is centered in the pipe at the beam injection end, 10,000 ft upstream, there is a slight slope which must be compensated for in the measurements.

Calculations

Survey, shop, and installation calculations were necessary for the alignment and placement of beam transport equipment. Each calculation required knowledge of the beam transport geometry calculated by TRANSPORT[11] and criteria defining the BSY inertial reference frame. This BSY reference

Figure 22-31 Laser alignment target stand in BSY.

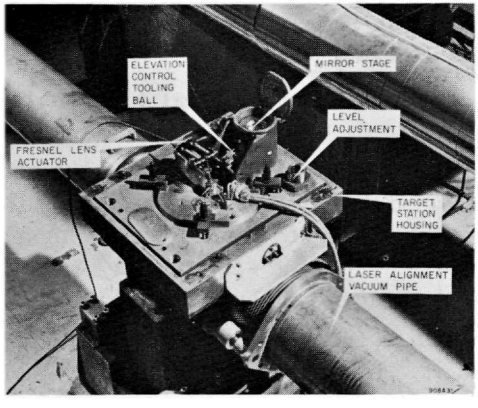

frame (see Fig. 22-30) is defined as follows. The Y axis is parallel to the gravity vector at accelerator station 105 + 08. The Z axis is in a vertical plane containing the accelerator axis and is perpendicular to the Y axis. The X axis is orthogonal to Y and Z. The origin of the system is at station 101 + 75.

Survey calculations preceded shop and installation calculations. Surveys were performed by SLAC and Aetron–Blume–Atkinson (ABA) to establish inertial reference points by creating both horizontal and vertical benchmarks.

Two computer programs, LAYOUT and VERTEX, were developed to compute the BSY component locations and alignment values. These programs were written with options so that equipment locations could be specified in both BSY or local gravity systems and redefined with respect to any previously defined points along any coordinate system. These options made possible the determination of tooling offsets and elevations required for the placement of targets on many of the components. Other computer programs were written to aid in field surveys, to reduce survey field data, and to analyze alignment data from the optical alignment shop.

LAYOUT and VERTEX had different input requirements. This difference insured independent analyses in providing the data. The drift lengths, bending angles in the beam plane, and desired options were required inputs for the VERTEX code. The usual input for LAYOUT was the TRANSPORT code deck used to compute the beam optics, plus other data cards which specified the desired coordinate system, the units, and the parameters of which the values were to be computed. This tie between the beam optics program and a component position program was desirable because it helped to eliminate human error in transcribing or making new data input cards, once the beam optics had been computed.

The A- and B-beam transport parameter values in the beam planes were computed by TRANSPORT. The expressions derived below show the relationships used to associate points in either beam plane to a common reference system, the BSY reference frame. In the beam plane, shown in Fig. 22-32, once an origin is specified, the beam transport parameters

Figure 22-32 Beam plane.

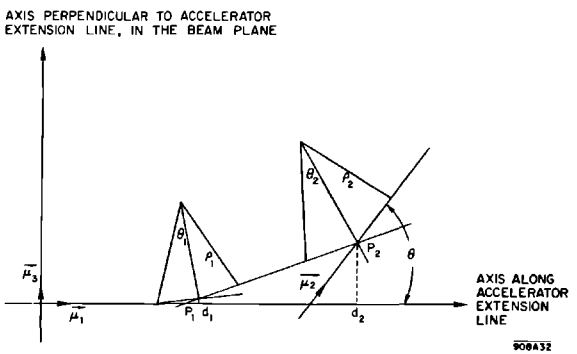

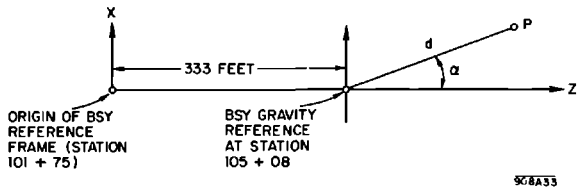

Figure 22-33
Definition of gravity vector parameters.

d_1, θ_1, ρ_1, d_2, θ_2, ρ_2, ... are sufficient to compute the coordinates of the vertices P_1, P_2, ... which define a beam line.

In vector notation, the position of any beam point can be expressed as a linear combination of two unit vectors, $\boldsymbol{\mu}_1$ and $\boldsymbol{\mu}_3$,

$$\mathbf{P}_i = x_i \boldsymbol{\mu}_3 + z_i \boldsymbol{\mu}_1 \tag{22-63}$$

where $\boldsymbol{\mu}_1$ lies along the accelerator extension line and $\boldsymbol{\mu}_3$ is perpendicular to $\boldsymbol{\mu}_1$ in the beam plane.

Then, if $\boldsymbol{\mu}_2$ is a unit vector along the beam exit line in the end station,

$$\begin{aligned} \boldsymbol{\mu}_1 \cdot \boldsymbol{\mu}_3 &= 0 \\ \boldsymbol{\mu}_2 \cdot \boldsymbol{\mu}_3 &= \sin\theta \end{aligned} \tag{22-64}$$

and

$$\boldsymbol{\mu}_1 \cdot \boldsymbol{\mu}_2 = \cos\theta$$

where θ is the angle between the beam exit line and the accelerator extension line. This angle is 24.5° for the A-beam and 12.5° for the B-beam. For the beam exit lines to be normal to local gravity in the end stations, one must have

$$\boldsymbol{\mu}_2 \cdot \mathbf{G}_y = 0 \tag{22-65}$$

where $\mathbf{G}_y$ is the local gravity vector.

In the BSY reference frame where unit vectors **i**, **j**, and **k** are taken along axes X, Y, and Z, the local gravity vector is

$$\mathbf{G}_y = \left(\sin\frac{d}{R}\sin\alpha\right)\mathbf{i} + \left(\cos\frac{d}{R}\right)\mathbf{j} + \left(\sin\frac{d}{R}\cos\alpha\right)\mathbf{k} \tag{22-66}$$

where d is the distance from station 105 + 08, and $1/R$ is the local earth curvature, 4.606×10^{-8} radian/ft. The angle α is defined as the angle between a line from station 105 + 08 to the point P being considered and the Z axis, as shown in Fig. 22-33, and is given by $\alpha = \arctan[x/(z - 333\text{ ft})]$.

Recalling that ϕ is the angle defined in Fig. 22-30, the beam entrance line into the BSY may be expressed as

$$\boldsymbol{\mu}_1 = -\sin\phi \cdot \mathbf{j} + \cos\phi \cdot \mathbf{k} \tag{22-67}$$

Expressions (22-63) through (22-67) may be used to solve for the beam vectors (μ_1, μ_2, μ_3) in terms of the BSY vectors (**i**, **j**, **k**) and thus to obtain the coordinates x, y, and z of a beam point P_i in the BSY reference frame. Equation (22-63) could then be expressed as

$$\mathbf{P}_i = x\mathbf{i} + y\mathbf{j} + z\mathbf{k} \tag{22-68}$$

Both LAYOUT and VERTEX programs used the above relationships to represent beam points in the various coordinate systems which were meaningful to the field, shop, and installation crews.

The external targets which were mounted on the BSY components were set so that the components are at the proper tilt when they are aligned. A mirror target was set on each component so that it is horizontal with respect to local gravity when the component lies in the tilted plane. This targeting procedure will be discussed later in this chapter under the section Shop Alignment.

One of the first required sets of calculations was that capable of supplying the information necessary to make the stretched wire layout shown in Fig. 22-34. The vertex monuments (VT) are the intersections of the beam drift lines entering and leaving a bending magnet group. The programs LAYOUT and VERTEX were used to find these intersection points. Once the values for the stretched wire layout were computed, the field crew required tape length values and elevation differences and offsets from these established lines.

The tape lengths required were the distances from VT to targets which had been placed on the components. These targets were usually preset mirror targets. The tape lengths set the position of the component along the beam. Because the field crews were familiar with possible obstructions for their tape pulls, the most workable procedure was found to be one in which these crews specified the respective monuments and components for which a tape distance was desired. This distance was then computed, checked, scribed on a tape, and given to the field crews for their use.

Figure 22-34 Vertex monument and stretched wire layout for alignment of BSY area.

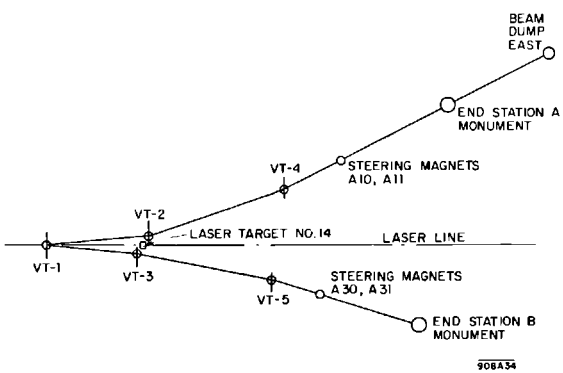

Elevation values for BSY components were computed in a sea level sense, i.e., concentric circles about the center of the earth, because survey crews follow the curvature of the earth with their level readings and sightings. However, to make the BSY a system independent of the earth, all elevation values were given as elevation differences between components. The tooling ball on laser target No. 14 near the center of the BSY was used as the inertial reference point for most elevation measurements.

SLAC tape bench

A tape bench facility was constructed at SLAC for scribing and calibrating the Invar field tapes. More than forty tape marks were scribed for the original equipment installation. Scribing accuracies within 0.003 in. were achieved. Although the actual placement of all components was not required to this accuracy, the gross errors due to tolerance accumulation were reduced by having all tape marks scribed on the tape bench.

The tape bench facility was built in a tunnel accessway in the accelerator housing. Double doors to the housing were installed and insulated so that the tape bench temperature stayed as constant as possible.

A monthly calibration check, made on each scribed tape, shows that the stability of the tapes after handling and general field use has been excellent. The maximum recorded deviation is less than 0.003 in. from the originally scribed length.

The standard tapes were 1200 in. long since most of the distance measurements made in the BSY fell within a 1200-in. range. As temperature stability is of primary concern with regard to mechanical measurements, Invar tapes were used because of the low thermal expansion of Invar. On the other hand, the stability of Invar under a continuous load is questionable; therefore, in order to keep the stress levels to a minimum, the tapes were allowed to hang in a catenary with just enough tension (10 lb) to keep the tapes off the ground over a 1200-in. span. Sometimes, allowing a survey tape to hang in a catenary with light tension can have detrimental effects on the measurements because air currents can cause the tape to vibrate. However, at SLAC, all the work requiring precision tape measurements was done in enclosed areas where wind was not a problem.

A series of tests were run to investigate the possible errors that might occur in long measurements because of creep of the Invar. The test periods were 5 days (120 hours) with the tapes under a 10-lb tensile load. The average stress level was 2000 psi, and the average ambient temperature was 70°F. The results of the tests indicated no measurable creep.

As the field survey tapes were to be used in a catenary configuration, it was necessary to have a calibrated standard tape which was held horizontal on the tape bench to correct for catenary sag. The standard was a graduated steel tape, calibrated by the National Bureau of Standards.

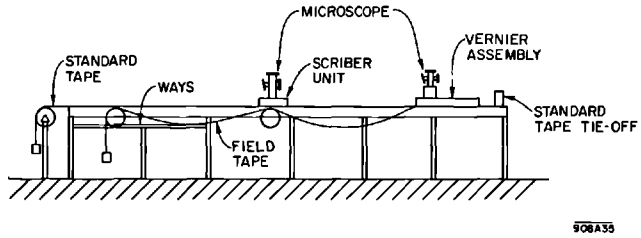

Figure 22-35 Schematic of the tape bench.

The tape bench (Fig. 22-35) consists of five major components: the vernier assembly, the scriber, pulleys, the standard tape, and the bench itself. Both the vernier assembly and scriber are equipped with microscopes for positioning the units over the desired location on the bench relative to the scribe marks on the standard steel tape.

The tape tie-off end of the bench is fabricated of aluminum jig plate which is approximately 10 ft. long. Gauge holes in this plate are set at 20-in. intervals and are used to locate the vernier assembly. These gauge holes correspond to the 20-in. increments of the steel master tape. The remainder of the bench is of hardwood with a steel framework. The entire length of the bench is supported by tubular members with adjustable bases for leveling purposes. These supports are spaced at 4-ft intervals.

The vernier assembly is an independent unit mounted on rollers which guide it along the tape tie-off end of the bench. The assembly has the capability of movement within the 20-in. gauge hole span from 0 to 24-in. increments of 0.0001 in. In this manner, the vernier assembly may be located at the desired 20-in. gauge hole location, and the independent slider mechanism may then be moved along until the desired scribing position is obtained. Attached to the assembly through a cable linkage is the end-supporting pulley for the Invar tape. The pulley is free to follow the travel of the vernier assembly.

The scribing unit mounted on a round steel way travels the full extent of the bench. The scriber houses a cutting tool mounted to the carriage containing the microscope. This tool marks the tapes once the scribing unit is in the desired location along the tape.

The pulleys are 16-in. diameter, $\frac{1}{2}$-in. thick, aluminum plates. Instrument-type ball bearings were used for mounting the pulleys on hardened steel shafts. The bearings were completely degreased and oiled with light clock oil. After mounting the pulleys on their respective shafts, they were balanced so that 1.6×10^{-3} lb applied at the diameter would rotate the pulley. This force is essentially a measure of the friction in the bearings. The net effect on the accuracy of the measurements is negligible since an error of 0.002 in. in an unsupported length of 1200 in. requires an uncertainty of 7×10^{-3} lb in the tension load.

The method for scribing tapes is to clamp the Invar tape into the vernier assembly so that the zero mark on the tape is immediately under the cross-hair reticule on the microscope. The free end of the tape is tensioned and supported over the pulley. The scriber is positioned by microscope over the correct 120-in. increment on the standard tape. The vernier assembly is then moved to the required interval between 0 and 120 in. on the steel standard so that the interval between the scriber and the vernier assembly on the standard is within 20 in. of the desired length. The fine adjustment is then made on the vernier such that the required span between the scriber and zero point on the Invar tape is obtained. The tape is clamped to the pulley on the scriber unit and scribed. The entire procedure is then repeated for calibration.

Support stands for the beam switchyard

Four different basic types of support stands are used in the BSY. These are the quadrupole magnet stands, the 3° bending magnet stands, the pulsed magnet stand, and the instrument stands. The bending magnet and quadrupole magnet stands are designed to support only one magnet. The pulsed magnet stand is required to support five pulsed magnets, six intervening protection collimators, two emergency dc magnets, and a pulsed vertical steering magnet. The instrument stands are designed with support rails so that they may support one or more interchangeable instruments. A few stands made by slightly modifying one of the four basic designs are used throughout the switchyard to accommodate special magnets or instruments.

The support stands are designed with fine adjustments to permit the final alignment of the components with six degrees of freedom, 3 translational and 3 rotational. The adjusting jacks can be operated from the second level of the BSY so that all alignment work can be done while the personnel are protected from residual radiation by a layer of concrete shielding.

Each support stand was designed to withstand specified earthquake shock loading and, of course, to support the BSY component which was to be placed on it. In the case of the 18-cm quadrupole magnet, a weight exceeding 17 tons must be supported.

The base supports for all stands use three jacks arranged in a tripod suspension. In the case of the magnet stands, the components rest on beds which are free to move in the plane determined by the three base jacks. Three other jacks are used to move the beds so that the stands have a total of six jacks to provide movement of the components placed on the stands. The jack design is a modification of the design which was made for the accelerator supports. These modifications increased the range and tightened the tolerances in backlash and translational motion of the jacks. The stands provide for a movement of ± 3 in. from the original center along any axis.

The major difference between the supports for the bending magnets and the quadrupole magnets is in the bed upon which the magnets rest. The

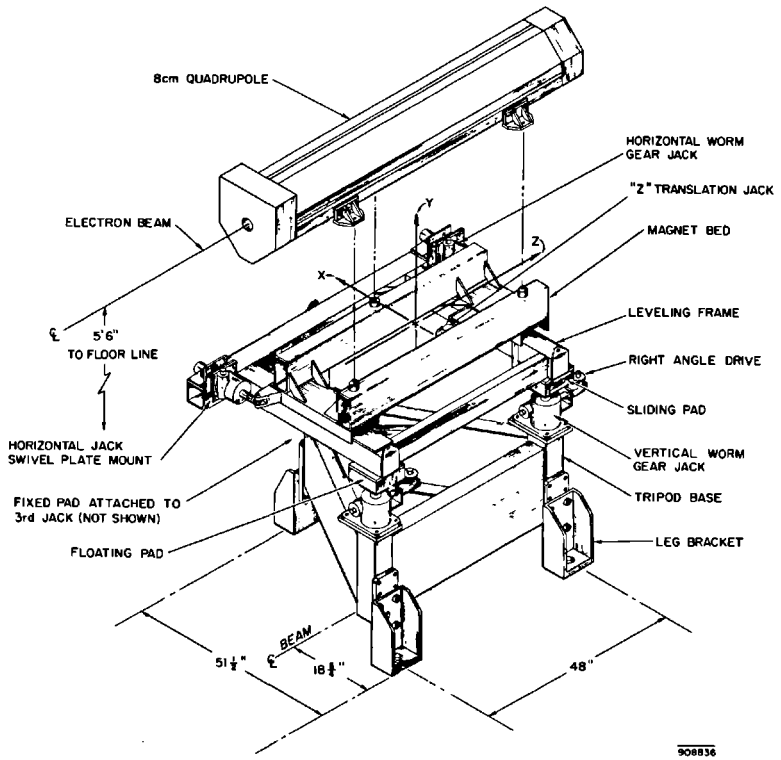

Figure 22-36 Support stand for 8-cm quadrupole magnet.

bending magnet support bed is flat while the quadrupole magnet support bed is in the form of a cradle in which the quadrupole magnet fits. A drawing of the support stand for an 8-cm quadrupole magnet is shown in Fig. 22-36.

The pulsed magnet stand is 44 ft long and supports all of the equipment from the downstream end of the high-power collimator to the beginning of the divergent vacuum chamber. Two laser targets are attached rigidly to the support frame for alignment of the stand in the switchyard. The pulsed magnets and the protection collimators which are also supported by the pulsed magnet stand are placed on reference pads on the stand. These pads are prealigned relative to the laser targets so that when the beam transport equipment is placed on the support and the support is aligned with the laser targets, the equipment is positioned in relation to the ideal beam location within about ± 0.04 in.

The instrument stands were built with level parallel rails instead of beds. The rails were accurately machined so that there are no deviations from straightness, flatness, or parallelism greater than 0.005 in. over their full length. The rails are located at a fixed distance below the electron beam so that instruments can be interchanged on the stands. The instruments are placed

on the rails in the shop and prealigned. The instrument stands cannot be translated along the beam axis and, thus, the stands have only five degrees of freedom; however, the instruments themselves may be moved on the rails so that their position along the beam may be adjusted.

Shop alignment

A special optical alignment shop was set up for the purpose of installing the external alignment targeting on the BSY components. All instruments and magnets that required targeting were processed through this shop before installation in the BSY. Tooling balls and mirror target assemblies were mounted on the exterior of the components to allow accurate installation with a minimum of effort on the part of the field installation crews.

The equipment in the alignment shop consisted of two 7-ft tooling bars and one 15-ft tooling bar, arranged in the form of a "T." The shop layout is shown in Fig. 22-37. Two fixed targets, the locations of which with respect to the tooling bars were precisely measured, were installed in the alignment shop. One was at the base of the "T" and the other under one of the arms of the "T." These targets are on the wall opposite the one shown in Fig. 22-37. They were used to set up a line of sight between the centers of the components to be aligned and the fixed targets. This line of sight simulated the electron beam path through the component during the alignment procedures. A stand with a permanently mounted telescope was installed at the intersection point of the "T." Being at the intersection, this telescope could be rotated to sight along any one of the tooling bars and could, therefore, be used for lining up other jig transits placed on the tooling bars. The transits on the tooling bars were aligned by autocollimation with the permanently installed telescope. A pair of high stands with a cross bar (see Fig. 22-37) were installed so that a jig transit could be placed directly over a component. The shop also contained an optical calibration stand with five collimators for aligning and checking the alignment instruments which were used in the shop and field.

Figure 22-37 Optical alignment shop.

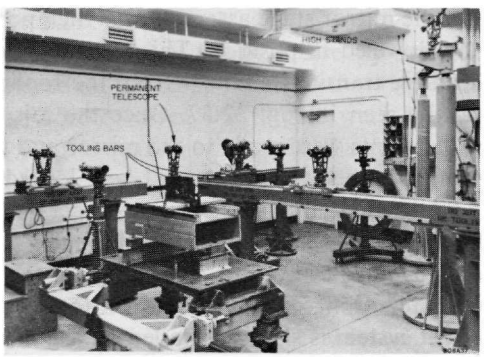

The optical alignment shop was located in a room which was built especially for alignment purposes. This room was in the Heavy Assembly Building where final assembly and magnetic measurement facilities were also located. The room for the alignment shop was constructed with a roof which had removable sections so that the components could be lowered in place and the roof sections could then be replaced. In this manner, the shop was kept relatively dust free and at a controlled temperature.

A magnet stand and an instrument stand were permanently installed in the alignment shop, one on each side of the long central tooling bar. A component to be aligned was placed on the appropriate stand so that the movable telescope on the long central bar could be used to make measurements along the beam axis (G_z axis) of the component. The telescopes on the shorter bars made measurements normal to the simulated beam path axis, i.e., along the component's G_x axis. Measurements along the vertical axis (G_y axis) were made by conventional leveling methods using precision spirit levels and optical tooling scales.

A component brought into the shop for alignment was first leveled and its mechanical or magnetic center located and marked. The exact determination of the centers of the components was important since all shop measurements, including those relating to location of targets for the components, were made using the centers as references. Special jigs were made to locate the mechanical centers. These jigs had a target attached to them so that when properly installed, the target was at the mechanical center. The magnetic centers of the quadrupole magnets were found by the use of a colloidal suspension of ferrosoferric oxide particles. The stand was then adjusted until the center and centerline of the magnet pole face were lined up with the fixed target on the shop wall and a jig transit which was held fixed on the stand at the other end of the magnet. The pole faces were leveled using precision levels and the secondary target tooling balls were then installed. Using the tooling bars, jig transits, a master level and scales, positions of the tooling balls were taken and recorded on the data sheet for the magnet. Then, using the center of the magnet as a rotation point, pitch and roll angles were turned into the magnet. This was accomplished by use of a clinometer, referenced to the leveled position with an accuracy of 2 arcsec or better.

The mirror stage assembly was then positioned on the magnet and bolted and doweled in position. This location was determined by use of the overhead jig transit positioned from the tooling bars. This overhead jig transit can be seen in Fig. 22-37. Once the mirror stage was fixed, final position adjustments were made to the mirror and the mirror leveled by autocollimation from the overhead transit, and locked in place.

A single stainless steel mirror target was used to control the position along the beam and the pitch and roll angles for the component. In conjunction with a bull's-eye target, the mirror also controls yaw. A single tooling ball mounted alongside the mirror on the vernier stage controls elevation. This target system is shown installed on a quadrupole magnet in Fig. 22-38.

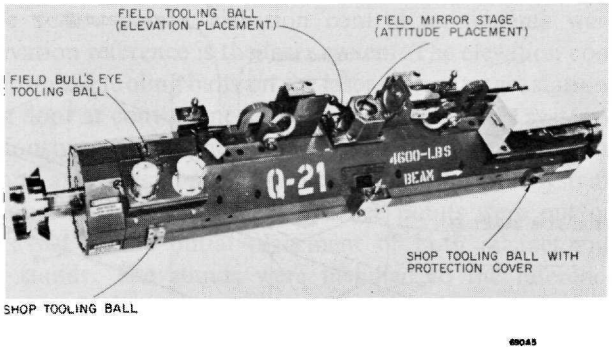

Figure 22-38 Alignment equipment on a quadrupole magnet.

The mirror target is mounted in an assembly called the mirror stage which consists of a series of gimballed cups which can be locked in a tilted position. The mirror has a reticule target etched on its surface face. The bull's-eye target is made from a 0.5-in. diameter stainless steel tooling ball. The ball has been ground flat on top and has concentric rings machined on the flat for a target.

Stainless steel is used for the bull's-eye and mirror targets because of its high corrosion and radiation resistance. A test was performed on a mirror target in which it was exposed to a 20% vapor solution of HNO_3 for 30 hours. After the test, the surface was discolored but the mirror was still useful and the reticule target was still discernible from the second level.

In addition to this primary target system for installation, a secondary system for checking alignment is also employed. It consists of three or four tooling balls, depending upon the component, located and doweled in position on the component. The position of these tooling balls is measured with respect to the mirror target and the tooling bull's-eye target with the component in the level position, and again in the tilted BSY position. With these measurements, the mirror target settings can be checked in the alignment shop and/or, if necessary, while in position in the BSY.

Wires were stretched along the second level of the BSY directly over the beam drift lines. The targets were placed on the components so that the alignment of the components would be correct when the targets were located directly under the stretched wires. On the instrument stands, the center line is obscured by the equipment and the targets had to be offset from center. The center line of the 3° bending magnets are not under the stretched wire. The offset distance from the drift line depends upon the position of the magnet in the bending group and its distance from the vertex point of the bend. Offsets from the magnet center line for the bending magnet mirror stages and tooling balls were computed for each magnet.

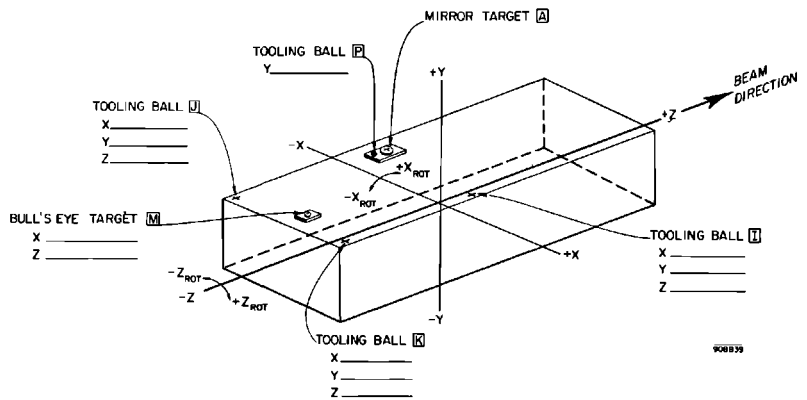

Figure 22-39 Alignment data sheet for a 3° bending magnet.

Shop installation procedures were written for each component to account for all of the above geometric requirements. A series of data sheets was made for each type of equipment to be aligned in the shop. These sheets had a drawing of the component showing the relative location of all alignment targets to be placed upon it. After the targets were installed, their positions were measured and entered on the data sheet. These sheets formed a valuable permanent record for the aligned component which can be used for checking the alignment, for realignment, and for making future changes to component location. A typical data sheet for the 3° bending magnet is shown in Fig. 22-39.

Installation alignment

Brass plates permanently fixed in the housing floor mark the vertex monument points. They are marked with a scribe to indicate their position relative to the laser system. Vertex point 2, VT-2, was set by trilateral measurement from two laser target stations. Because of its close proximity to the center of the BSY, VT-2 served as control point for the establishment of the remaining vertex points throughout the BSY. The other vertex points were defined by trilateral measurement between VT-2 and one of the laser target stations most accessible for horizontal measurement.

In order to align the equipment beyond the final vertex points, VT-4 and VT-5, turning points were established at the steering magnet groups, some 70 ft downstream from each of these vertex points. Since the electron beam was to be steered into the end stations by these magnets, their locations could be used as secondary alignment monuments. To reduce long pulls of the stretched wire, these groups of steering magnets were used as one of the tie-off points. From the end station steering magnet groups, the wires were extended across the end station monuments, thus defining the theoretical beam drift path into the end stations.

In addition to the vertex points, elevation control monuments were required. The basic elevation reference is the laser system. The elevation controls were transferred from the tooling balls on the laser system target stations to rivets in the housing floor at convenient points for both transport systems.

As described previously, each magnet and beam diagnostic instrument was assigned a horizontal and vertical position in the beam transport system. The component positions were surveyed and reference points were put on the housing floor to assist in the initial placement of both magnet and diagnostic instrument stands. The stands were installed to the reference points so that a minimum of adjustment would be required during the final alignment process.

The layout of the BSY was designed so that the optical alignment could be performed through penetration holes in the shielding, corresponding to the alignment targets on the components. Holes were also placed in the shielding to permit operation of the jacks on the alignment stands. Figure 22-40 gives a view of the second-level operation.

The field installation of all components is very similar. The description of the installation of a bending magnet given below should make the installation and field alignment of any component clear. A schematic view of the setup for a magnet is shown in Fig. 22-41. Jig transits are plumbed over the vertex points upstream and downstream of the magnet. A steel wire, 0.004 in. in diameter, is then stretched between the two vertex points. The wire is supported at either end on an adjustable table and is then moved until it

Figure 22-40 Second-level alignment of BSY component.

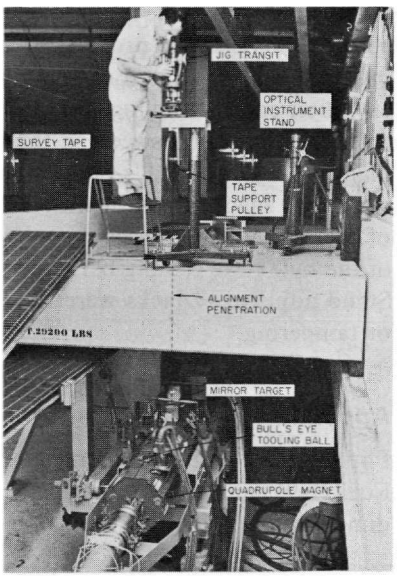

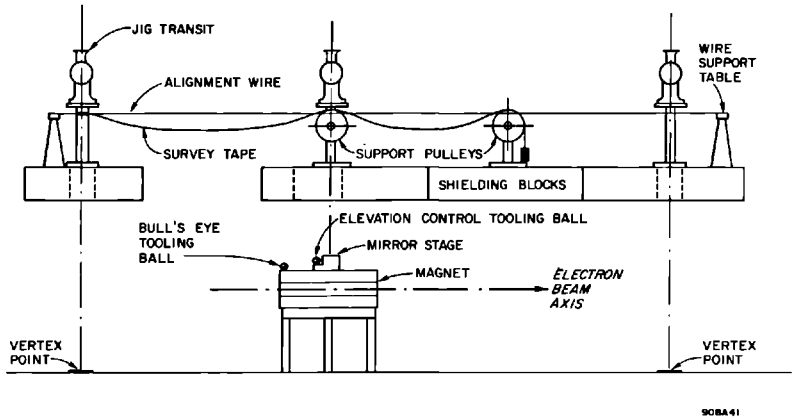

Figure 22-41 Schematic layout of installation alignment setup.

bisects the line of sight of the jig transits. This wire now lies over the theoretical beam drift path through the series of components between the two vertex points. A survey tape is extended over a pulley support system parallel to the stretched wire. The tape defines the horizontal location of the magnet along the beam drift path from one of the vertex points. A third jig transit is plumbed directly over the wire at the scribe mark on the survey tape corresponding to the location of the magnet mirror target.

The component was correctly positioned by making the mirror target coincident with the line of sight of the jig transit and the tape scribe mark. This placed the center of the mirror target directly under the alignment wire. The magnet was then adjusted to autocollimate the transit on the mirror target thus making the mirror perpendicular to the line of sight. This operation gave the magnet the proper tilt to make it parallel to the beam plane. The magnet was then set for elevation by reference to a sight rod set on the elevation control tooling ball on the magnet mirror stage. The correct yaw rotation was set by sweeping the jig transit along the wire and rotating the magnet until the bull's-eye tooling ball was directly under the alignment wire. The magnet was then in its proper position. Final checks were made of the autocollimation of the mirror, the magnet elevation, and the position of the bull's-eye tooling ball and mirror stage center line relative to the wire. Stand adjustment jacks were then lock-wired to prevent further adjustment or tampering.

Appendix: maximization of intensity (MJL)

For a target pattern having alternate slots and ribbons, the integrals in Eq. (22-9) can be written as sums of integrals over the slots. Consider two-dimensional vectors

$$\mathbf{V}_n = (C_n(0), S_n(0))$$

with

$$C_n(0) = \int_{\mu_{n-}}^{\mu_{n+}} \cos\left(\frac{\pi}{2} t^2\right) dt$$

and

$$S_n(0) = \int_{\mu_{n-}}^{\mu_{n+}} \sin\left(\frac{\pi}{2} t^2\right) dt$$

In terms of these vectors, the peak intensity is given by

$$I(0) = \left(\frac{A}{2l}\right)^2 I_\mu I_v$$

where

$$I_\mu = |\mathbf{V}|^2 = \left|\sum_n \mathbf{V}_n\right|^2$$

with a similar expression for I_v. Thus, in order to optimize the peak intensity, the length of the vector V must be maximized.

A procedure for maximizing |V| will be illustrated graphically. On a plot of the Cornu spiral, start from a point μ_{1-}, which corresponds to a given central ribbon width of a target, and draw a straight line through the end point of the spiral, E, as in Fig. 22-42. The points of intersection of the

Figure 22-42 Cornu spiral used to show graphic method of determining the optimum target design. The point μ_{1-} corresponds to the edge of the central ribbon. Subsequent slot edges correspond to the intersections of successive curves of the spiral with the line joining E and μ_{1-}.

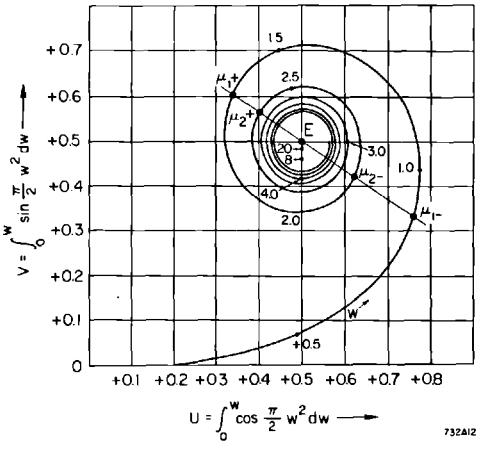

line with the spiral constitute a set of μ_{n+} and μ_{n-} which maximizes $|V|$. It can be seen that each of the vectors $\mathbf{V}_n$ has an optimum length and all vectors lie along the same direction.

It can be shown analytically that the values of μ_{n+} and μ_{n-} are approximately given by

$$\mu_{n\pm} = (4n - d \pm 1)^{1/2}$$

with

$$d = 3 - \mu_{1-}^2$$

where

$$\mu_{1-}^2 = \frac{lw^2}{2\lambda rs}$$

in which w is the width of the central ribbon.

For this, it suffices to show that the slopes of the lines joining $\mu_{n\pm}$ and E are independent of n.

From Eqs. (22-16) and (22-17), the slopes of the lines joining $\mu_{n\pm}$ and E are

$$M_{\pm}(d) = \frac{\left[\dfrac{\sin[(\pi/2)\mu_{n\pm}^2]}{\pi\mu_{n\pm}^2} - \cos\left(\dfrac{\pi}{2}\,\mu_{n\pm}^2\right)\right]}{\left[\dfrac{\cos[(\pi/2)\mu_{n\pm}^2]}{\pi\mu_{n\pm}^2} - \sin\left(\dfrac{\pi}{2}\,\mu_{n\pm}^2\right)\right]}$$

from which

$$M_{\pm}(d) = \frac{\sin[\pi/2(d \pm 1) - \phi]}{\cos[\pi/2(d \pm 1) + \phi]}$$

where

$$\phi = \tan^{-1} \pi\mu_{n\pm}^2$$

Because $d < 3$, $\pi\mu_{n\pm} > 12$ for $n \geq 2$ so that $\phi \approx \pi/2$. Hence,

$$M_{\pm}(d) = \frac{\sin \pi d/2}{\cos \pi d/2}$$

which, being independent of n, proves that the choice of edges is optimized.

Acknowledgments

The authors of this chapter wish to recognize SLAC's director, W. K. H. Panofsky, for his key part in developing the basic concepts of the Fresnel target system. The accelerator assembly and installation work was directed by D. Robertson and C. Rasmussen. The Fresnel lens system was tested and calibrated by O. Turpen. The early design of the switchyard alignment system was made by J. Voss. The BSY assembly and installation work was directed

by H. Weidner and R. O'Keefe. The targeting and field alignment of BSY components was directed by B. Hooley, E. Head, and W. Walsh. One of the computer programs used for BSY alignment was written by S. Howry. Many other workers were needed in all these areas. The contributions of all of them and the cooperation of their department heads is hereby gratefully acknowledged.

References

1 F. A. Jenkins and H. E. White, *Fundamentals of Optics*, 3rd Ed., McGraw-Hill, New York, 1957.

2 K. R. Trigger, "Approximate Solutions of Images Using Fresnel Zone Plates," Rept. No. SLAC-TN-64-19, Stanford Linear Accelerator Center, Stanford University, Stanford, California (1964).

3 Max Born and Emil Wolf, *Principles of Optics*, pp. 428-434, Macmillan, New York, 1964.

4 *Ibid.*, p. 122.

5 *Ibid.*, p. 88.

6 R. Sandkuhle, "Support Girder Fabrication," Rept. No. SLAC-TN-67-24, Stanford Linear Accelerator Center, Stanford University, Stanford, California (1967).

7 K. Skarpaas, "Elasticity Theory and Design of Flexible Supports for Stanford Two-Mile Linear Accelerator," Rept. No. SLAC-TN-67-9, Stanford Linear Accelerator Center, Stanford University, Stanford, California (March 1967).

8 J. K. Cobb and J. J. Murray, *Nucl. Instr. Methods* **46**, 99-105 (1967).

9 H. S. Butler, S. K. Howry, and C. H. Moore, "Specifications for the Beam Transport Systems to End Stations A and B," Rept. No. SLAC-29, Stanford Linear Accelerator Center, Stanford University, Stanford, California (1964).

10 R. E. Taylor, *IEEE Trans. Nucl. Sci.* **NS-12** (No. 3), 84 (June 1965).

11 H. S. Butler, S. K. Howry, and C. H. Moore, "TRANSPORT ... A Computer Program for Designing Beam Transport Systems," Rept. No. SLAC-DOC-12, Stanford Linear Accelerator Center, Stanford University, Stanford, California (1964).

12 A. Kilert, "Position Tolerances for Equipment in the Beam Switchyard," SLAC Engineering Note 000-014, Stanford Linear Accelerator Center, Stanford University, Stanford, California (1966).